JAERI-M
85-080

JAPANESE CONTRIBUTIONS TO IAEA INTOR WORKSHOP, PHASE TWO A, PART 2

CHAPTER VIII : PHYSICS

July 1985

Tatsuoki TAKEDA, Teruaki SHOJI, Shin YAMAMOTO, Norio SUZUKI, Tomonori TAKIZUKA, Tadanori MIZOGUCHI*[1], Masayuki NAGAMI, Kazuo KAWAHATA*[2], Masayoshi SUGIHARA and Noboru FUJISAWA

日 本 原 子 力 研 究 所
Japan Atomic Energy Research Institute

JAERI-Mレポートは，日本原子力研究所が不定期に公刊している研究報告書です。
入手の問合わせは，日本原子力研究所技術情報部情報資料課（〒319-11茨城県那珂郡東海村）あて，お申しこしください。なお，このほかに財団法人原子力弘済会資料センター（〒319-11茨城県那珂郡東海村日本原子力研究所内）で複写による実費頒布をおこなっております。

JAERI-M reports are issued irregularly.
Inquiries about availability of the reports should be addressed to Information Division Department of Technical Information, Japan Atomic Energy Research Institute, Tokai-mura, Naka-gun, Ibaraki-ken 319-11, Japan.

編集兼発行　日本原子力研究所
印　　刷　㈱高野高速印刷

Japanese Contributions to IAEA INTOR Workshop, Phase Two A, Part 2 Chapter VIII : Physics

Tatsuoki TAKEDA[+1], Teruaki SHOJI[+1], Shin YAMAMOTO[+1], Norio SUSUKI[+1], Tomonori TAKIZUKA[+1], Tadanori MIZOGUCHI[*1], Masayuki, NAGAMI, Kazuo KAWAHATA[*2], Masayoshi SUGIHARA and Noboru FUJISAWA

Departmant of Large Tokamak Research
Naka Fusion Research Establishment, JAERI

(Received May 31, 1985)

This report corresponds to Chapter VIII of Japanese contribution report to IAEA INTOR Workshop, Phase Two A, Part 2. Data base assessments are made for stability limits, confinement, neutral beam heating and current drive, operation scenario, and burning plasmas. R & D programme and impacts on INTOR design are specified.

Keywords: INTOR, Beta Limit, Density Limit, Disruption, Energy Confinement, Particle Confinement, Momentum Confinement, Neutral Beam Heating, Neutral Beam Current Drive, Operation Scenario, Alpha Confinement, Burn Control, Tokamak, Assessment

---

+1 Department of Thermonuclear Fusion Research

*1 Hitachi Ltd.

*2 Institute of Plasma Physics, Nagoya University

IAEA INTOR ワークショップ
フェーズⅡA，パート2 報告書
第Ⅷ章：物理

日本原子力研究所那珂研究所臨界プラズマ研究部
竹田 辰興[+1]・庄司 昭朗[+1]・山本 新[+1]
鈴木 紀男[+1]・滝塚 知典[+1]・溝口 忠憲[*1]
永見 正幸・川端 一男[*2]・杉原 正芳
藤沢 登

（1985年5月31日受理）

この報告書はIAEA主催のINTORワークショップ，フェーズⅡA，パート2の日本の報告書の第Ⅷ章に相当するものである。安定限界，閉込め，中性粒子入射加熱と電流駆動，運転シナリオ，燃焼プラズマに関するデータベースの評価を行なった。研究開発のプログラムとINTOR設計へのインパクトについても考察している。

＋1 核融合研究部
＊1 （株）日立
＊2 名古屋大・プラズマ研究所

Contents

目　　次

1. Stability Limits

1.1 Physics design assumptions and parameters (Phase IIA)[1]

During the Phase IIA Part I of the INTOR workshop, experimental and theoretical data on the beta limits of a tokamak plasma accumulated considerably. Experimental results obtained up to the Phase IIA Part I are summarized as follows: (1) the present beta limit is soft one but saturation of the beta value with increasing heating power is clearly observed in many devices, (2) the highest beta value of $\langle\beta\rangle$=4.6 % was attained in the Doublet III experiments, and (3) the high poloidal beta value as $\varepsilon\beta_p\sim2/3$ is attained, which is a little larger than the INTOR design value of $\varepsilon\beta_p\sim0.6$. As for the theoretical progress on the beta limit the ideal MHD stability theory is converging and some features of the beta scaling are being clarified, but the issues still remain controversial, especially, implication of instability modes on the beta limit is not clear. And also there are serious questions if the averaged beta $\langle\beta\rangle$ of 5.6 % is really attainable with the present design parameters of the INTOR and what is a reliable beta scaling law applicable to design a large tokamak with a higher beta value. Efforts to obtain the reliable beta scaling law and to establish a scenario to higher beta state are necessary.

The density limit is improved by various technological progresses such as vacuum processing of a chamber, high power heating, or appropriate fuelling technique. The design value of average ion density of the INTOR is $1.4\times10^{20}m^{-3}$. The Murakami parameter of the highest beta discharge in the previous Doublet III experiment is slightly larger than the INTOR design value. However, the mechanism of the density limitation and the scaling law of the density limit are not well understood theoretically and the solution of this issue remains for future extensive analyses.

Many new experimental results on disruptions in ohmic heating regimes were obtained during the period covered by the Phase IIA Part I workshops. Many of them are consistently understood within the framework of the previously obtained knowledge on the mechanism and characteristics of the disruptions. In general the disruptions occur, phenomenologically, in a plasma with too low safety factor q_s, too high rising speed of density dn/dt, or too high density n. In some devices such as Doublet III and TFR the disruption evolutions were investigated minutely. The detailed time history seems different from a device to another. Theoretical studies have not been able to clarify the comprehensive picture of the disruptions yet. Therefore, the important information for the INTOR design, such as the frequency of occurence of disruptions, time scale of plasma decaying process, and spatial and temporal heat deposition profiles remains unclear and experimental information up to now cannot be extrapolated to the parameter range of the INTOR plasma. It was concluded in the summary of the workshop that present knowledge is not sufficient to specify a disruption control system for the INTOR and more research is necessary on all aspects of disruption including the question of why disrupting equilibria develop and how this can be avoided.

1.2 Data Base

1.2.1 Beta limits

1.2.1.1 Experimental status

Since the last summary of the INTOR workshops (Phase IIA Part I) there seems no remarkable progress in the experimental studies on attaining higher beta equilibria. But steady accumulation of experimental data continues and these data obtained by various tokamaks seem to behave similarly in broad outlines[2,3].

As for the effort to attain a higher beta equilibrium, extensive studies on the low q_s discharges under the condition of a relatively low toroidal field were continued in Doublet III from the viewpoint that the higher beta value could be attained for the lower q_s discharge[4]. In order to attain the very-low-q stable discharge in the Doublet III ramping of the plasma current during the NBI heating is effective[5]. By the technique the plasma with safety factor as low as 2 and 1.5 were obtained for the plasmas with large ($0.41<a<0.44$) and small ($0.34<a<0.38$) minor radii, respectively. In these experiments the maximum beta values are 3.3 % and 4.5 % in the respective order. An extensive effort to get higher plasma pressure, i.e., a high beta value at higher toroidal field strength has been also made. In the series of the experiments the volume average beta of about 2 % is obtained for the toroidal field of 2.2 T, where $T_e(0)\sim 5keV$, $T_i(0)\sim 5.5keV$, $n_e>6.5\times 10^{13}cm^{-3}$, $\beta(0)\sim 6.4\%$ with $\sim 8MW$ NBI heating[6].

1.2.1.2 Theory

Among theoretical problems it is very important to clarify the mechanism of the beta limitation of the tokamak plasma and to establish a reliable scaling law of the beta limit (the critical beta value β_c). At present quantitative discussion on the beta limit is possible only within the framework of the MHD stability analyses, sometimes with taking into account of modification by kinetic effects. In the following we summarize the four topics on the stability analyses which relate to the beta limit of the tokamak plasma, i.e., the analyses of the infinite-n ballooning mode, the finite-n kink mode, the beta scaling law due to the modes, and the finite-n ballooning modes.

<Infinite-n ballooning mode>[7,8]

In general a growth rate of a higher-n mode is higher and infinite-n ballooning modes are considered to play the most crucial role on the limitation of the plasma pressure. These instabilities are sensitive to the shape of the plasma cross section, pressure anisotropy, pressure profile, and current profile. In order to obtain a high beta equilibrium stable against the infinite-n ballooning modes, optimization with respect to these parameters is required.

The basic equations used for the optimization of the pressure profile against the infinite-n ballooning mode are the combination of the axisymmetric equilibrium equation (Grad-Shafranov equation),

$$R\frac{\partial}{\partial R}\left(\frac{1}{R}\frac{\partial\psi}{\partial R}\right) + \frac{\partial^2\psi}{\partial Z^2} = -R^2\frac{dp}{d\psi} - T\frac{dT}{d\psi}, \qquad (1.2.1.1)$$

and the ballooning mode equation with zero growth rate (the marginally stable ballooning mode equation),

$$\frac{d}{ds}\left(f\frac{d\varphi}{ds}\right) + \frac{dp}{d\psi}\Big|_c g\varphi = 0, \qquad (1.2.1.2)$$

$$f = \frac{1}{R^2 B_p}\{1 + (\frac{R^2 B_p^2}{B} z)^2\} ,$$

$$g = \frac{1}{B^2 B_p}\{\frac{\partial}{\partial \psi}(2p + B^2) - \frac{R B_t B_p}{B} z \frac{\partial B^2}{\partial s}\} ,$$

$$z = \int_0^s \frac{ds}{J B_p} \frac{\partial}{\partial \psi}(\frac{J B_t}{R}) ,$$

where ψ and T are the poloidal flux function and the toroidal magnetic field function, respectively, and s and J are the arc length of the magnetic field line projected on the meridian plane of the torus and the Jacobian of the co-ordinate system. The above equation is simply derived from the usual infinite-n ballooning mode equation by setting ω=0 and it is solved as an eigenvalue problem with the eigenvalue of $\lambda(\psi)=dp/d\psi|_c$ (critical pressure gradient). By employing the marginally stable ballooning mode equation high accuracy analyses can be carried out with less CPU time of the computer systemin comparison with the usual method where the squared growth rate ω^2 is calculated as an eigenvalue of the system. The optimization procedure is as follows; (1) a certain equilibrium is prepared with a given safety factor profile $q(\psi)$, (2) the Grad-Shafranov equation is solved for a given pressure profile $p(\psi)$ under the adiabatic constraint $p(\psi)(dV/d\psi)^\gamma=const.$, where V and γ are the volume surrounded by a magnetic surface and the ratio of specific heat, (3) the marginally stable ballooning mode equation is solved and the critical pressure profile $p_c(\psi)$ is calculated from the eigenvalue profile $\lambda(\psi)$ of the equation, (4) the pressure profile $p(\psi)$ for the Grad-Shafranov equation is replaced by the critical one $p_c(\psi)$. And the processes (2)-(4) are repeated. When the difference between p and p_c becomes small, the iteration is terminated and we obtain the equilibrium marginally stable against the infinite-n ballooning mode in the whole plasma region.

Since stability of the ballooning mode is sensitive to the plasma shape (A: aspect ratio, κ: ellipticity, δ: triangularity), pressure profile $p(\psi)$ and safety factor profile $q(\psi)$ optimization with respect to these parameters is required to realize a stable high beta equilibrium. Azumi et al. optimize the pressure profile for an equilibrium with given shape of the plasma surface and given q-profile[7]. In these analyses, q-profile is given by a force-free equilibrium with the toroidal current profile, $j_\varphi=D(1-\psi)^\alpha/R$, ($\psi$: normalized poloidal flux function). The values of D and α are adjusted such that the safety factor at the magnetic axis, q_0, and that at the plasma surface, q_s, take prescribed values.

The dependence of the critical beta value β_c on the safety factor at the plasma surface q_s is studied in the wide range of the ellipticity κ and the triangularity δ of the plasma cross section. Figure 1.2.1.1 shows the q_s dependence of β_c for different value of κ and δ in a tokamak with the aspect ratio A=3.375. The safety factor at the magnetic axis q_0 is unity. The triangular deformation of the elliptic tokamak increases the critical beta value considerably, especially, in the low q_s region. By fits on the numerical results, Takizuka got the following formula of the critical beta value for q_0=1[8],

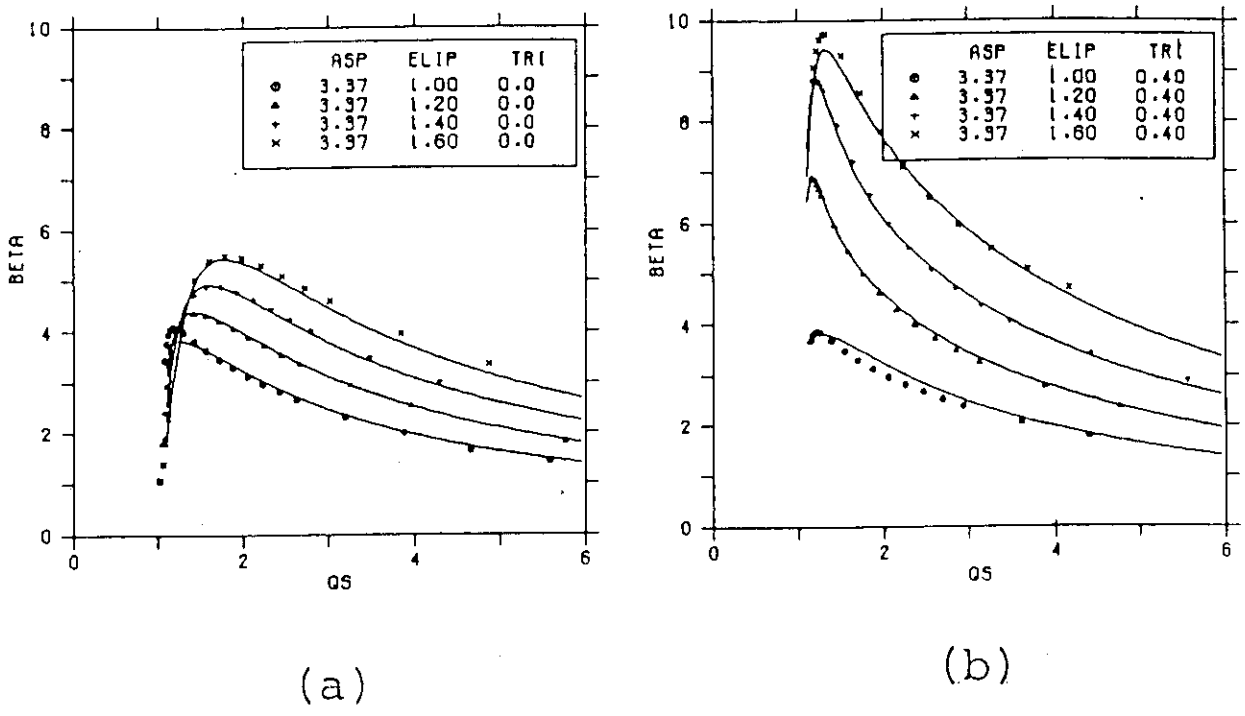

Fig.1.2.1.1 Dependence of the critical beta β_c on q_s for equilibria with A=3.375. Safety factor at the magnetic axis q_0 is fixed at 1.0. (a) δ=0, and (b) δ=0.4.

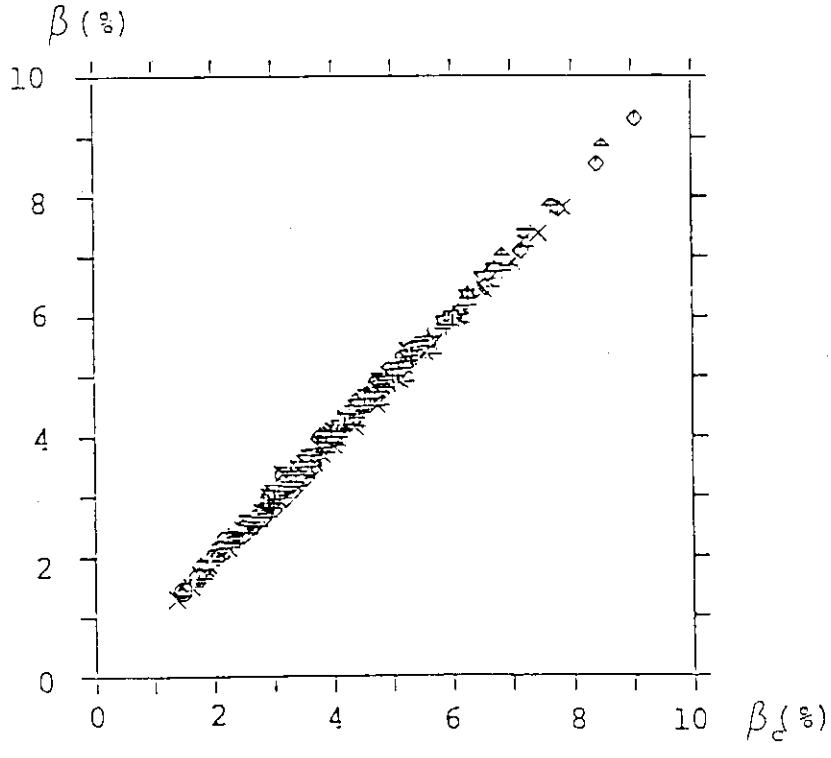

Fig.1.2.1.2 Critical beta value for infinite-n ballooning mode. Numericalluy obtained beta β is well represented by β_c (eq. (1.2.1.3)).

$$\beta_c(\%)=\frac{30\kappa^{1.5}}{Aq_s}\{1+0.9(\kappa-1)\delta-0.6\frac{\kappa^{0.75}}{q_s}+14(\kappa-1)(1.85-\kappa)\frac{\delta^{1.5}}{q_s^4}\}. \qquad (1.2.1.3)$$

Figure 1.2.1.2 shows that numerically obtained critical beta values β are well represented by the above formula(β_c). Elongation and triangular deformation cooperatively increase the critical beta value. In evaluating the critical beta value it should be noted that the safety factor q_s for finite beta considerably deviates from that of a cylindrical plasma with noncircular cross section. For optimized equilibria, the relation between q_s and the total plasma current I_p is approximately given by

$$\frac{1}{q_s}=A\sqrt{(1-1/A^2)}\,(\frac{2}{1+\kappa^2}-0.08\delta)\frac{\mu_0 I_p}{2\pi a B_{t0}}-0.07\{1+(\kappa-1)\delta\}, \qquad (1.2.1.4)$$

where a is the plasma minor radius and the MKS unit is used. It should be noted that, in the equation, $1/q_s$ is not proportional to I_p because the equation is derived for the series of marginally stable equilibria and the constant term corresponds to the beta effect on the equilibria. Improvement of the critical beta value by the large triangular deformation becomes less effective as the ellipticity κ decreases and the triangularity does not help to improve a circular cross sectional tokamak as seen from the term $(\kappa-1)\delta$ in eq.(1.2.1.3). The result is different from the scaling law obtained by Bernard et al.[9] which shows that the critical beta value is improved by the triangularity even for small κ and large q_s. This combined effect of the ellipticity and triangularity on the improvement of critical beta value comes from the large modification of the local shear (Fig.1.2.1.3).

Another important result of the new analysis is the dependence of the critical beta value on q_0. Figure 1.2.1.4 shows the q_s dependence of β_c for different values of q_0 for κ=1.6, δ=0.4, and A=3.375. The critical beta value can be increased by increasing q_0. This improvement of β_c by large q_0 is also strongly related with the triangular deformation of the plasma cross section and the increase of q_0 reduces the critical beta value for a purely elliptic tokamak, as expected by the theoretical prediction. It is, however, suspicious if the large q_0 operation really helps to improve the limiting beta value in a practical situation. This problem will be considered again in relation with the finite-n kink mode analyses.

In order to investigate the infinite-n mode comprehensively Itoh et al. analyzed the kinetic instability by employing the high-n approximation keeping the effect of the toroidal shift[10]. Due to the wave-particle interaction this mode is unstable in the first as well as the second stability regions of the MHD stability diagram. Figure 1.2.1.5 shows the growth rate vs. beta value for the parameters: L_N/R=0.1 ($L_N^{-1}=|\nabla N/N|$), q=3.2, rq'/q=1, $T_e=T_i$, $k\rho_i$=0.2, n=0.063a/ρ_i (solid line) and $k\rho_i$=0.5, n=0.16a/ρ_i (broken line). The change in the growth rate does not occur abruptly at the MHD critical beta value. The higher-n modes are especially affected by the finite gyroradius effect. For $k\rho_i$=0.5 ($n\sim$50 for $a/\rho_i\sim$300), MHD growth rate does not exceed ω_* and the growth rate reduces as the density increases. The middle-n mode may set the most serious barrier to the second stability region.

In summary optimized high beta equilibrium stable against only the infinite-n ballooning mode is obtained by choosing simultaneously high

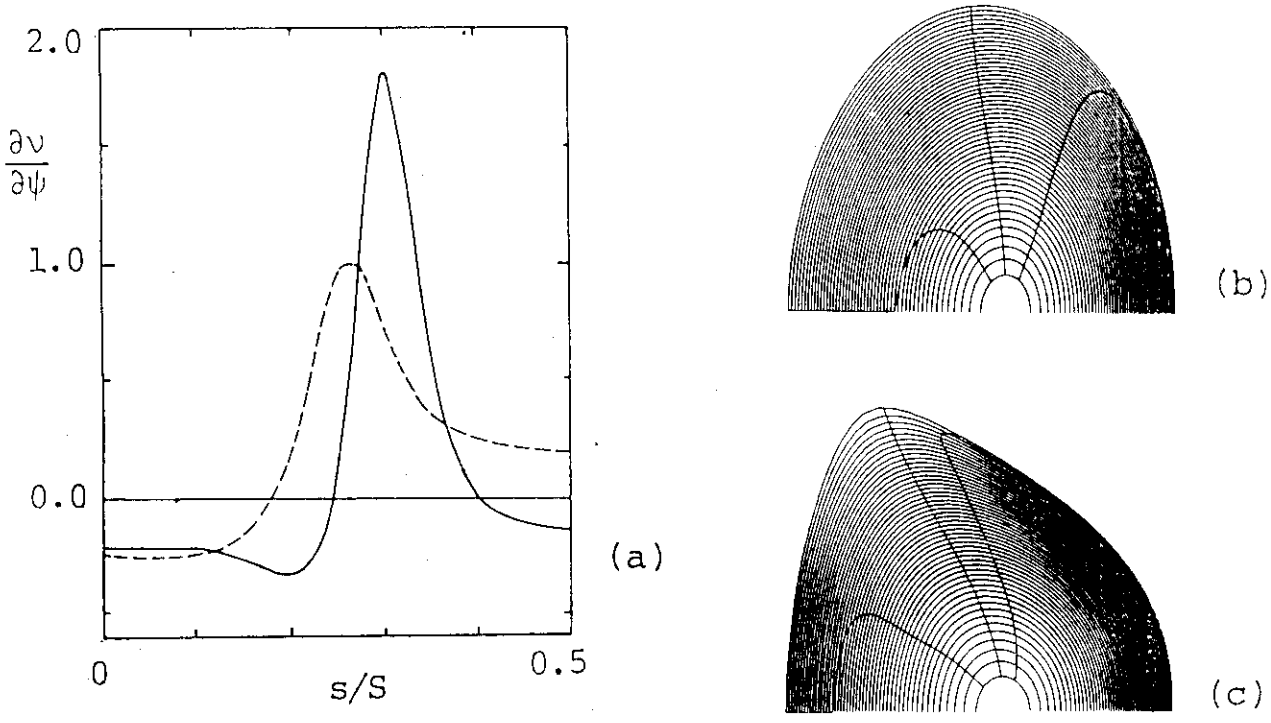

Fig.1.2.1.3 Local shear ($\partial\nu/\partial\psi$) distribution in elliptic ((b) and solid line in (a): δ=0) and D-shaped ((c) and broken line in (a): δ=0.5) plasmas. Negative local shear regions are below the left and right curves in the subfigures (b) and (c). Subfigure (a) shows local shear distribution on a magnetic surface ψ/ψ_s=0.5. Negative local shear at the outside of the torus has stabilizing effet for the ballooning mode and it is clearly shown that the stabilizing zone expands in the D-shaped plasma in comparison with the circular plasma. The equilibria are for A=3.375, κ=1.6, q_0=1.0, and q_s=2.0.

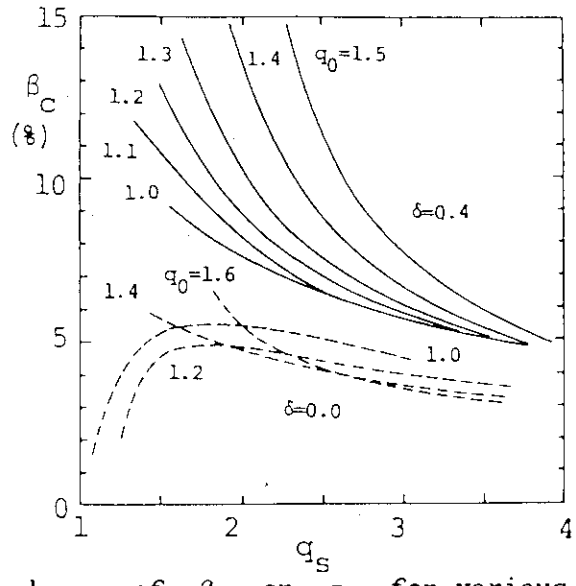

Fig.1.2.1.4 Dependence of β_c on q_s for various values of q_0, where A=3.375 and κ=1.6.

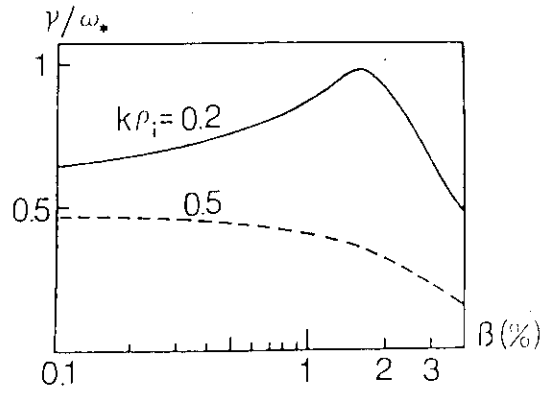

Fig.1.2.1.5 Growth rate vs. β of the high-$n$kinetic ballooning mode obtained by the high-n approximation for $k\rho_i$=0.2 (solid line) and $k\rho_i$=0.5 (broken line).

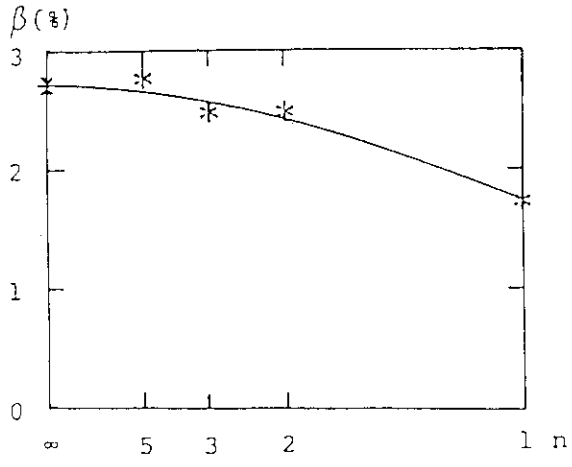

Fig.1.2.1.6 Mode number dependence of the critical beta value against the free boundary mode for A=3.38, κ=1, δ=0, q_0=1, and q_s=2.6.

κ, high δ, high q_0, and low q_s. It is very important to investigate whether this kind of optimized equilibrium is accessible or not. Further studies are necessary on other kinds of instabilities by taking into account of the transport and/or heating processes. The result of the kinetic analyses shows that the transition between the stability and instability regions of the MHD modes is smooth and suggests the soft beta limit. But conclusion on the implication of the instability on the beta limit requires more extensive analyses of infinite- and finite-n modes including 3-dimensional nonlinear simulations[8].

<Finite-n kink mode>[8]

Free boundary modes remain unstable for the optimized equilibria against infinite-n balloonig mode. By using the ERATO code[11] Tsunematsu et al. studied the stability of the free boundary modes for the same equilibria as those for the infinite-n ballooning mode. Figure 1.2.1.6 shows the dependence of the critical beta on the mode number n for the case of no conducting wall. The n=1 kink mode is the most unstable and the beta limit for n>1 is almost the same as that for the infinite-n ballooning mode. Therefore, we study the beta limit of the n=1 kink mode. The dependence of β_c for the n=1 kink mode on κ, δ and q_s is shown in Fig. 1.2.1.7 for A=3.38 and q_0=1. Similar calculation for equilibria with higher q_0 shows considerable degradation of kink mode stability and we only consider equilibria with q_0=1 in this paragraph. The points along the dashed and the solid lines correspond to the cases of high shear ($3<q_s<4$) and the low shear ($2<q_s<3$), respectively. The wall stabilization is a recipe to increase β_K without the degradation of the beta limit due to ballooning mode, if a first wall of a fusion reactor plays the role of a conducting wall[7,11]. In our cases β_K almost coincides with β_B when the conducting wall is placed at a_w/a=1.5 (a_w: minor radius of the wall)(Fig.1.2.1.8).

The formula for the critical beta against the n=1 kink mode is expressed similarly as in the case of the infinite-n ballooning mode as

$$\beta_c(\%)=\frac{C\kappa^{1.65}}{Aq_s}\{1+(\kappa-1)\delta\} \qquad C=14\ (2<q_s<3)\ \ and\ \ C=20\ (3<q_s<4),$$

$$\beta_c\sim 0 \qquad for\ \ q_s<2, \qquad (1.2.1.5)$$

where inverse proportionality on the aspect ratio is assumed. This formula has the similar form to the dominant terms in eq.(1.2.1.3) for $q_s>2$, and eq.(1.2.1.4) almost holds in this case too.

<Practical scaling laws>[8]

Though the scaling law of eq.(1.2.1.3) may be used as an excellent guide line to design an ambitiously high performance tokamak reactor, this form of the expression is not necessarily convenient to apply to the design study of a standard tokamak reactor. In deriving a more convenient expression it should be, especially, noted that the critical beta value is approximately proportional to the plasma current in a practical or conservative tokamak (Fig.1.2.1.9). This tendency is also observed in the case of the n=1 kink mode. And both of the equations for the ballooning and kink modes are roughly expressed in the range of $q_s>2$ by using the total plasma current I_p as

$$\beta_B(\%)=(20\pm 2.5)\mu_0 I_p/(2\pi a B_{t0}) \qquad \text{for ballooning mode,} \qquad (1.2.1.6)$$

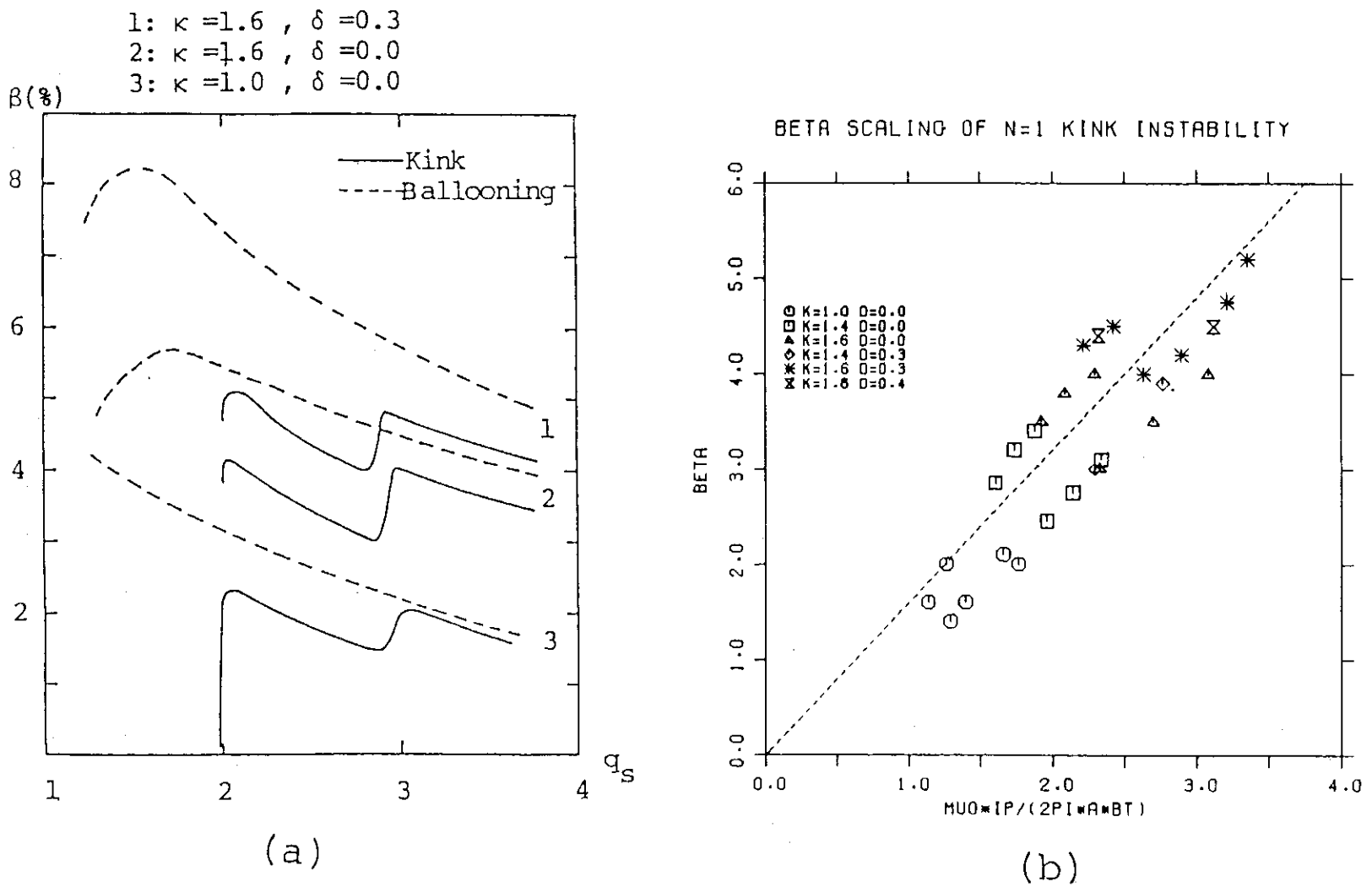

Fig.1.2.1.7 The dependence of β_c for the n=1 kink mode on κ, δ, and q_s for A=3.38 and q_0=1. (a) The dependence of β_c as a function of q_s. (b) The dependence of β_c as a function of the normalized current. The points along the dashed and solid lines correspond to the cases of high shear ($3<q_s<4$) and the low shear ($2<q_s<3$), respectively.

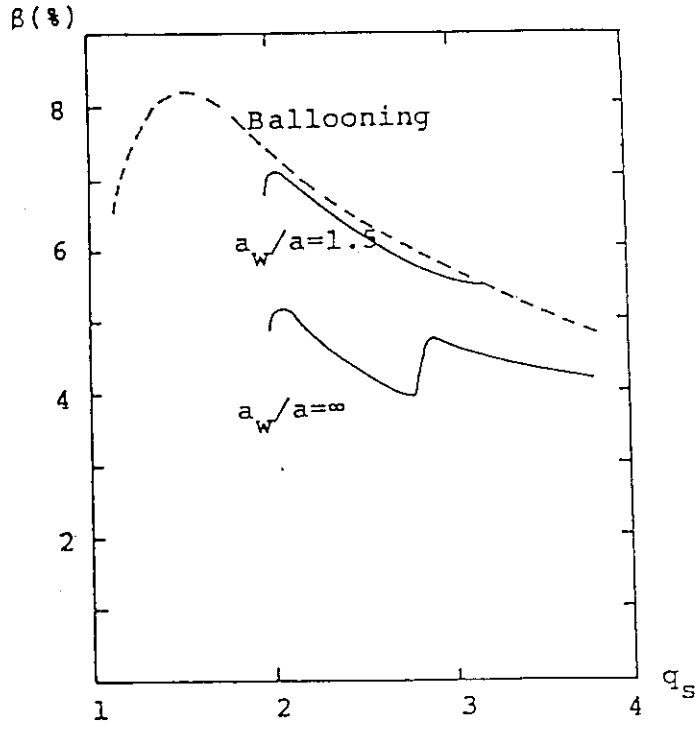

Fig.1.2.1.8 Improvement of the critical beta against the n=1 kink mode by the wall stabilization. Plasma parameters are the same as those of Fig.1.2.1.7.

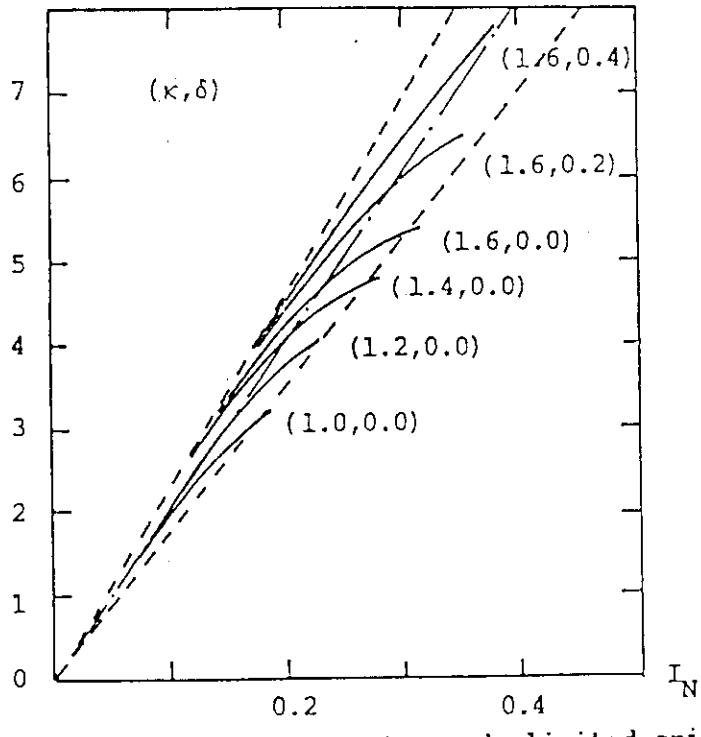

Fig.1.2.1.9 The dependence of the ballooning-mode-limited critical beta on the normalized plasma current $I_N=\mu_0 I_p/(2\pi a B_{t0})$. Solid lines are drawn according to the numerically obtained scaling formula (eq.(1.2.1.3)). Between two dashed lines the safety factor at the plasma surface is restricted within 2 and 3.

$$\beta_K(\%)=(16\pm2.0)\mu_0 I_p/(2\pi a B_{t0}) \quad \text{for } n=1 \text{ kink mode.} \qquad (1.2.1.7)$$

The coefficients in eq.(1.2.1.7) are almost the same as those obtained by other calculations[13,14]. The n=1 kink mode tends to be unstable because j_φ remains finite at the plasma surface due to the feature of the optimization procedure of the pressure profile. If we choose the q-profile with sufficiently decreasing current profile near the plasma surface, β_K increases with the decrease of β_B and two beta limits will become closer.

<Finite-n ballooning modes>[15]

These modes are studied numerically by using the revised version of the ERATO code[11] in which the quasi-mode representation is incorporated and middle-n modes could be analyzed comparatively easily. However, systematic parameter survey of the finite-n ballooning modes still consumes a lot of CPU time and only typical cases are studied and qualitative results are obtained as for the feature of high beta equilibria of a tokamak plasma[15]. As examples of the low-, middle-, high-n ballooning modes Tsunematsu et al. studied the n=3, 10, and 50 modes, especially, to find the second stability region and investigate the dependence of the stability of ballooning modes on pressure profiles. The series of the FCT(flux conserving tokamak) equilibria with a peaked pressure profile (case 1: $\Delta p=S(1-\psi)^2$) and a flat profile (case 2: $\Delta p=S(1-\psi^4)^4$) are examined by fixing the ratio representing the magnetic shear, q_s/q_0 = 2.5.

The stability diagrams for n=3, 10, and 50 modes are shown in Fig.1.2.1.10. For the equilibrium with flat pressure profile, the n=3 mode is always stable and n=10 mode has the second stability region for the poloidal beta value above 2.2. On the other hand, the n=50 mode is unstable above a critical poloidal beta value ($\beta_p>1.1$ for both the peaked and flat pressure profiles) and there is no second stability region. The figure shows also that there is no second stability region around $q_0=1$ for the case 1, whereas the equilibrium for the case 2 has that of n=10 mode for $q_0>1$. The broken line in the figure is the stability limit for the infinite-n ballooning mode. The n=50 mode for the case 2 has very narrow second stability region around $q_0\sim1.75$ and $\beta_p>1.6$, while the mode for the case 1 has no such a region.

In order to find out a guide line for the optimization of the equilibrium, the potential energy contributions are evaluated by classifying them as the Alfvén term (A), ballooning term (B), and kink term (K) in the total potential energy (W). Figures 1.2.1.11(a) and (b) show the poloidal averaged terms for the cases 1 and 2, respectively, when n=10 and β_p=2.2. The peaked pressure profile can cause broad convective motion in the plasma column. In the flat pressure profile equilibrium the stabilizing Alfvén term exceeds the ballooning term. The mode is more localized near the plasma surface. The existence of the second stability region of the middle-n ballooning modes depend on the pressure profiles. The figures also show that the kink term has the same order of magnitude as the ballooning term for middle- to low-n mode as $n\sim10$. Therefore, optimization of the current profile remains still effective for the stabilization of the middle- as well as low-n modes. Also it seems that the external kink mode will be a beta limiting instability after the optimization with respect to the finite-n ballooning modes is carried out.

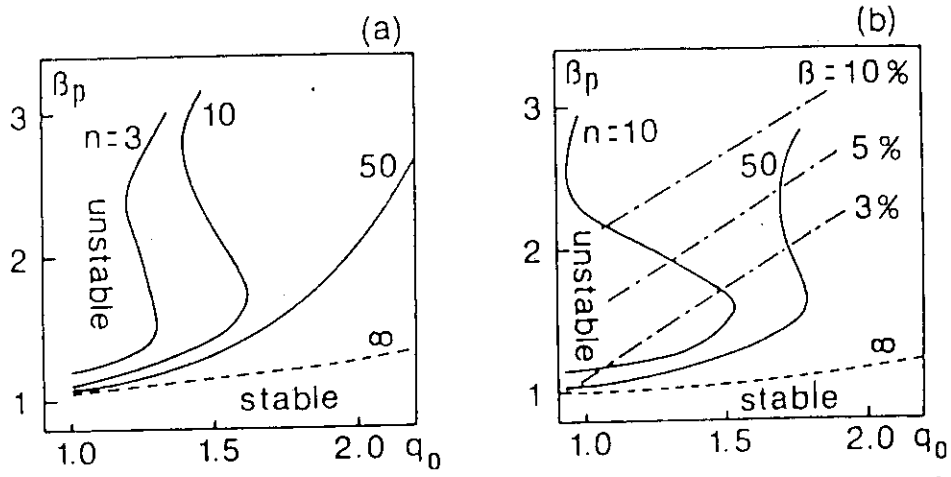

Fig.1.2.1.10 Stability diagram of the finite-n ballooning modes in (q_0,β_p) plane for (a) case 1 and (b) case 2. Left side of a line is the unstable region of each mode. The n=3 mode for case 2 is stable when q_0>1. Broken line is stability limit of the infinite-n ballooning mode.

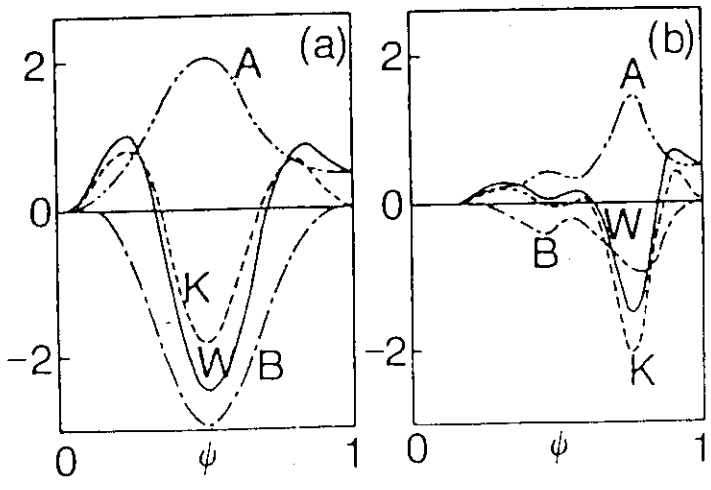

Fig.1.2.1.11 Potential energy of n=10 mode normalized to kinetic energy for case 1 with β_p=2.2 (a) and for case 2 with β_p=2.2 (b).

In addition to the analyses of the finite-n ballooning modes of an isotropic pressure plasma effect of the pressure anisotropy on the stability of the finite-n ballooning modes was also studied[16]. Among various possibilities of the pressure anisotropy the following simple anisotropic pressure equilibria are chosen for the stability analyses,

$$\Delta^*\psi = -\frac{R^2}{\sigma}\frac{\partial p_\parallel}{\partial \psi} - \frac{1}{2\sigma^2}\frac{\partial}{\partial \psi}(\sigma T)^2 - \frac{1}{\sigma}\nabla\psi\nabla\sigma \ , \qquad (1.2.1.8)$$

$$\sigma = 1 + \frac{p_\perp - p_\parallel}{B^2} \ ,$$

$$B = \left(\frac{|\nabla\psi|^2}{R^2} + \frac{T^2}{R^2} \right)^{1/2} .$$

The tensor-pressure ERATO (TERA) was applied to the problem for the above equilibria and the stability diagram was obtained as shown in Fig.1.2.1.12 for the n=10 ballooning mode. For the above types of pressure profile the stabilization effect of the anisotropic pressure $\varepsilon\alpha$ $(=(p_\parallel - p_\perp)/(p_\parallel + p_\perp))$ is expected in the low β_p and low q_s equilibrium because the inward shift of average pressure surface is large in the outside region of the torus. However, parameter survey on the mode number and different types of the pressure anisotropy is lacking and further extensive investigation is necessary to judge whether the anisotropic pressure helps or not to attain a high beta state in a practical tokamak reactor.

1.2.1.3 Comparisons and conclusions

We obtained scaling laws which give the accessible beta value of tokamaks by the optimization of the pressure profile against infinite-n ballooning mode and by stability analyses of finite-n free boundary modes for the optimized equilibria. The scaling laws are expressed by eqs.(1.2.1.3) and (1.2.1.5) for infinite-n ballooning mode and for n=1 kink mode, respectively. These scaling laws are roughly expressed as $\beta_c = \hat{C}I_p$ for q_s>2. This kind of parameter dependence is predicted by several theoretical groups in the world and the coefficient of the scaling law are summarized in Table 1.2.1.1[8,9,13,14]. The comparison between this theoretical prediction and experimental data obtained up to now is presented in Fig.1.2.1.13. From this figure it seems rather difficult at present to attain a high beta state above the theoretically predicted limit. And it seems reasonable that the equation $\beta_c = \hat{C}I_p$ gives a practical beta scaling law for a standard tokamak of the present day.

1.2.2 Density limits

1.2.2.1 Experimental status

Density limit of a tokamak is well represented by the DITE plots, where operational regimes with high density and low safety factor are clearly shown together with the advancement of the used experimental techniques. Results of JAERI tokamaks (DIVA[16], JFT-2[21], JFT-2M[22], Doublet-III[20]) are shown in Figs.1.2.2.1 - 1.2.2.4. DIVA had a Cu shell and a poloidal divertor, and Ti gettering was used. By limiter discharges in DIVA with ohmic heating, high density and low q plasma was attained. The Murakami parameter of 5.2×10^{19} $m^{-2}T^{-1}$ was reached. JFT-2

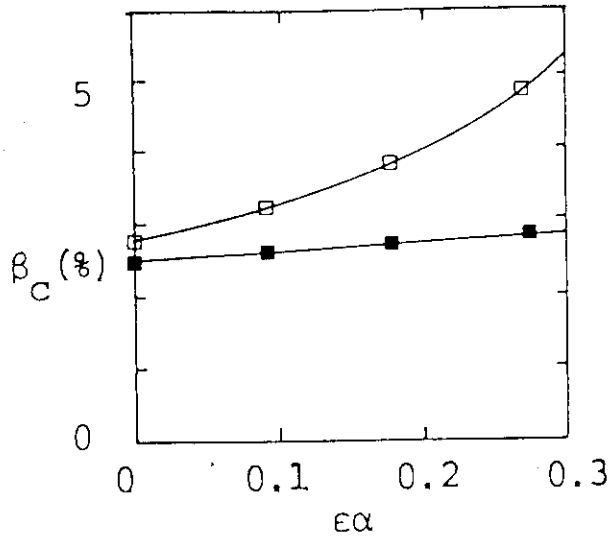

Fig.1.2.1.12 Dependence of the critical beta β_c for n=10 ballooning mode on pressure anisotropy $\varepsilon\alpha$. Open and black squares denote low shear (q_s/q_0=1.5) and high shear (q_s/q_0=2.5) equilibria, respectively.

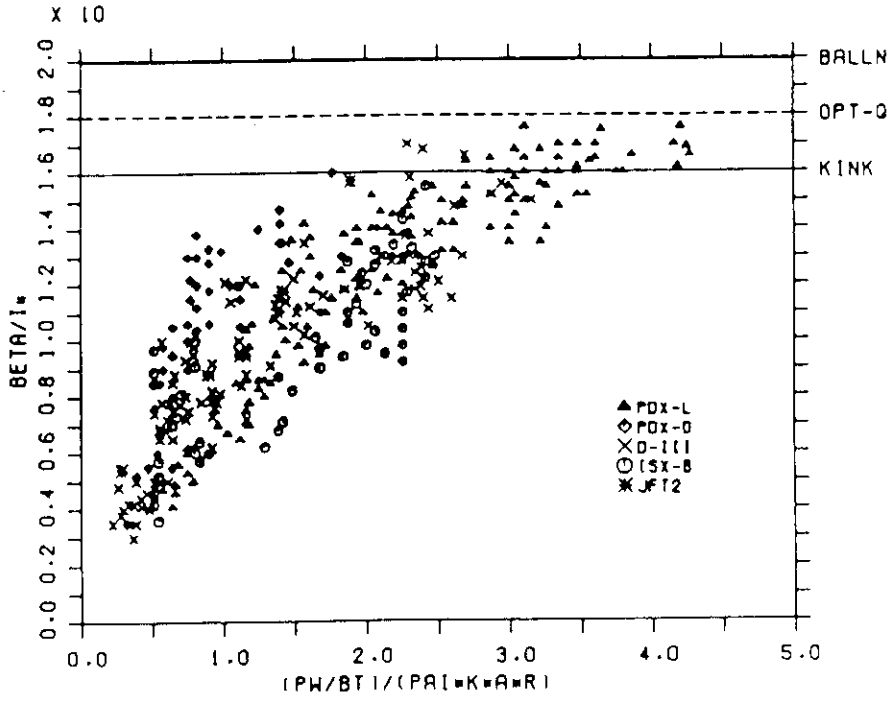

Fig.1.2.1.13 Comparison of the experimental data and the theoretical predictions of the beta limit.

Table 1.2.1.1 Coefficients of the beta scaling laws obtained by different authors. Coefficient C of the equation $\beta_c = C\mu_0 I_p/(2\pi a B_{t0})$ is shown where the MKS unit is employed.

	BALLOON	KINK
JAERI	20+-2.5	16+-2.0
CRPP		14
FOM		27
CULHAM	22	
GA	14.5	

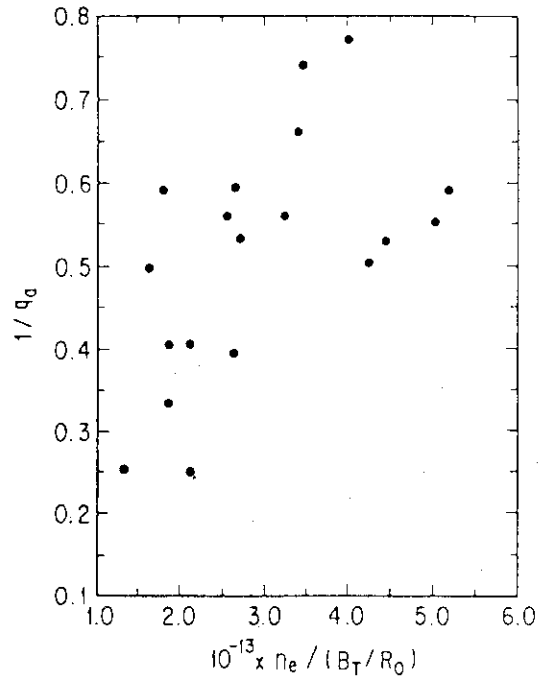

Fig.1.2.2.1 DIVA operational regime in the DITE plot, where units of n_e, B_t, and R_0 are cm^{-3}, T, and m, respectively.

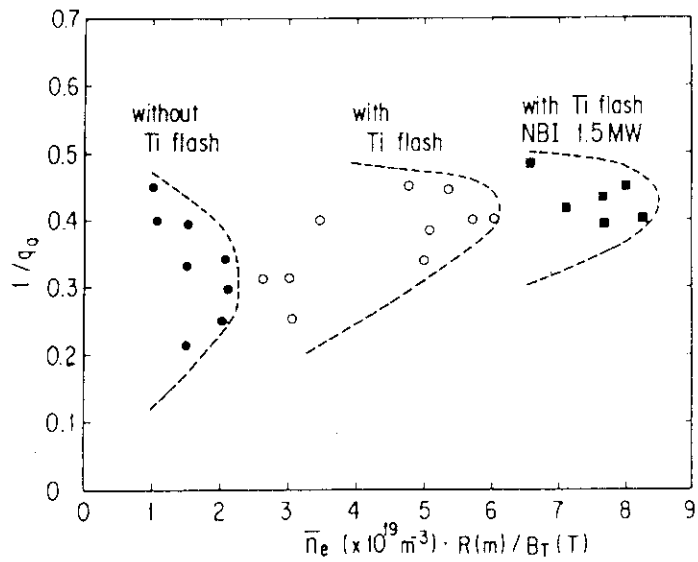

Fig.1.2.2.2 JFT-2 operational regime in the DITE plot, where units of n_e, B_t, and R_0 are cm^{-3}, T, and m, respectively.

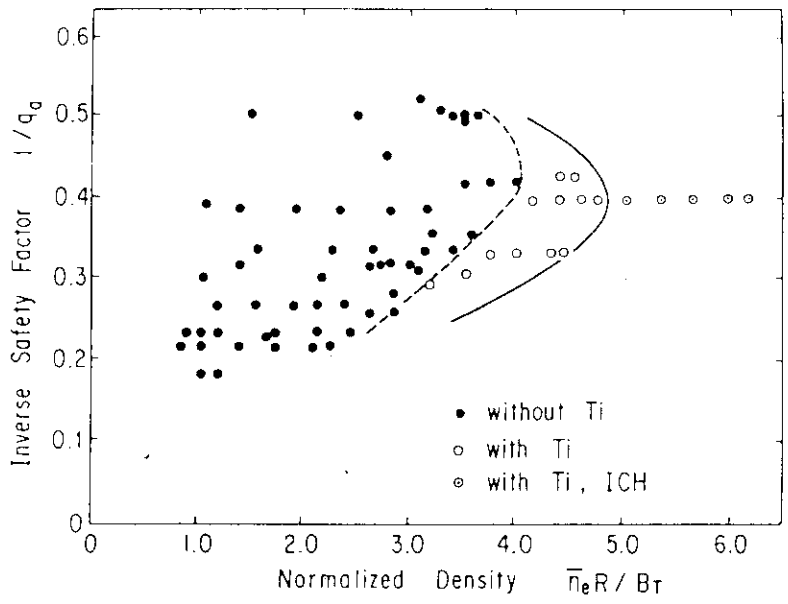

Fig.1.2.2.3 JFT-2M operational regime in the DITE plot, where units of n_e, B_t, and R_0 are cm^{-3}, T, and m, respectively.

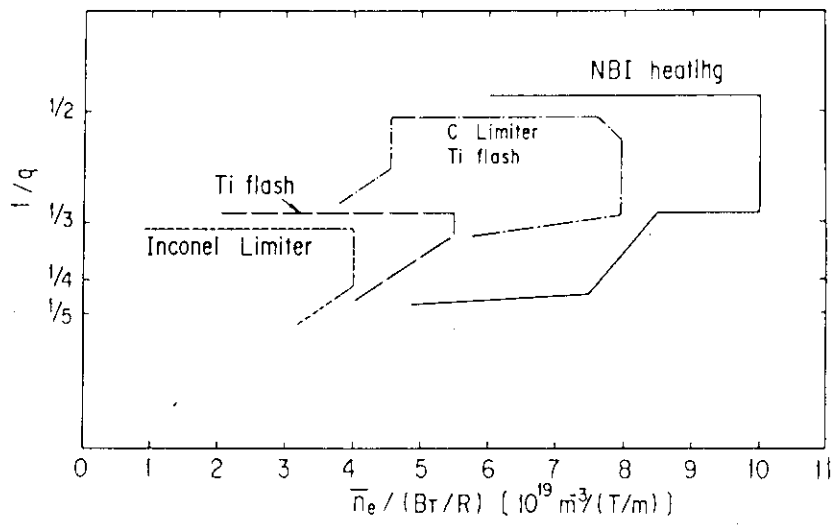

Fig.1.2.2.4 Doublet-III operational regime in the DITE plot, where units of n_e, B_t, and R_0 are cm^{-3}, T, and m, respectively.

was a circular tokamak without a shell. The density limit in the device was improved gradually by Ti gettering and NBI heating, finally the Murakami parameter of $9.0\times10^{19}\ m^{-2}T^{-1}$ was obtained. JFT-2M has a D-shaped vacuum vessel and now density limit is being improved by Ti gettering and additional heatings. Up to now, the Murakami parameter of $6.5\times10^{19}\ m^{-2}T^{-1}$ is obtained with 1.2 *MW* ICRF heating. In Doublet III, JAERI team has carried out experiments on high density and low q discharges. Wall conditioning with TDC and Ti gettering and choice of TiC coated graphite as limiter material have resulted in the highest Murakami parameter of $10\times10^{19}\ m^{-2}T^{-1}$ with NBI heating.

Experiences obtained through these studies are as follows: (1) The Murakami scaling[21] of density on B_t/R is effective to describe the operational regimes of a tokamak plasma the Murakami parameter well represents cleanliness of the plasma. Clean vacuum condition is one of necessary conditions to obtain a high density plasma, because the ratio of radiation loss rate to input power has some threshold value. In ohmic heating, it lies at 40 - 80 %. (2) In ohmic heating without Ti gettering, the Murakami parameter lies in $2 - 4\times10^{19}m^{-2}T^{-1}$ and with Ti gettering in $4 - 8\times10^{19}m^{-2}T^{-1}$. Additional heatings increase the value up to $6 - 10\times10^{19}m^{-2}T^{-1}$. The ratio of radiation loss to inputpower has a tendency to take a lower value in the case with additional heatings. (3) In order to obtain a high density and low q plasma, careful programming of the plasma current and gas puffing rate, and appropriate position control are necessary. If it is not the case major disruption terminates the discharge.

1.2.2.2 Theory

1.2.2.3 Comparisons and conclusions

1.2.3 Disruptions

1.2.3.1 Experimental status

(i) Major disruption

We have not yet reached a comprehensive even phenomenological description of the disruption by which we could logically classify the variety of existing experiments. The important informations needed to understand and overcome the disruptions are: conditions for the disruptions, detailed description of the time evolution, frequency, heat deposition profiles, and density and current limitations. Experiments aiming at developing techniques to increase density and to lower q_s values are also closely relating topics. One of the very important questions concerning the mechanism of the major disruption is what kind of the MHD modes exist and whether the modes are external or internal ones. Experimental observations are conveniently classified from this viewpoint. In the following we summarize the experimental results on the disruption obtained by the Japanese scientists' group(Table 1.2.3.1).

During the previous phase of the INTOR workshop, a systematic study of the disruptions was carried out in DIVA[17]. The results obtained in the series of the experiments are summarized as follows: (1) after reducing impurities no major disruption was observed, (2) by injection of neon gas at q_s=2.5, radiation loss increased and the disruption was excited, (3) m=2/m=1 precursor oscillation was observed before the disruption and for the plasma with q less than 2 disruption did not

Table 1.2.3.1 Experimental findings on the disruptions by the Japanese scientists' groups.

DISRUPTIONS

Device	Year	Reference	Condition	Diagnostics	Observation	Evolution	Remarks
JFT-2a (DIVA)	1979	Nucl. Fusion 20 (1980) 271	$q_a>2$	*MHD activity *1D tokamak code Tearing code	*Various 2/1 Low level 3/2 *No disr. for $q_a<2$ *I: no effect	2/1+int. disp. →major disr.	Low impurity b/a=1.2 → q_a=1.3
JFT-2	1979	J. Phys. Soc. Japan 48 (1979) 273	$q_a\sim3$ impurity high density $q_a<2$	*MHD activity *Shell effect	*3/1,2/1 modes *b/a=1.8 → q_a=1.7 *b/a=2.4 → q_a=1.9	2/1+1/1 →major disr. 2/1 → major disr.	Low impurity
JIPP T-I (1)	1982	Nucl. Fusion 22(1982)465	Current ramp. Gas puff.	*T_e prof. → (code) → J prof. → (code) → Island evol. *MHD activity		*2/1+3/2 → soft *2/1+limiter → soft *2/1+3/2+limiter → hard	J profile control (puff, I ramping) Position
JIPP T-I (2)	1983	JIPP-630		*MHD activity *Island measure.		*Impurity → 2/1+3/2 → →narrow J prof. → 1/1 → 2/1→ asym. reconn.	
Doublet-III (1)	1982	Nucl. Fusion 22(1982)409	$q_a\gtrsim2$ Current ramp. Gas puff. Ohmic heating		*Small stable window for gas through.		Low impurity Position control Slow ramp. Puff control
Doublet-III (2)	1983	unpublished	$q_a<2$ Current ramp. Gas puff. NBI heating		*Both internal & external modes possible from equilibrium calculation		High density by I ramp.+ NBI heating

appear. These results seem to confirm the disruption scenario of the nonlinear tearing mode origin. On the other hand the experiments carried out in JFT-2 tokamak suggested that the disruption is caused by the m=2 kink mode[22]. Regrettably, however, further investigations were not carried out within the JFT-2 experimental program.

After these experimental studies two series of experiments concerning the disruption phenomena in JIPP T-II were published. The first series of experiments were carried out by Toi et al.[23] In the series of the experiments various phenomena associated with the standard types of disruptions, i.e., negative voltage spikes, development of MHD activities with various mode number, sudden decrease of the plasma temperature, and termination of the discharge were observed. The authors calculated the width of the magnetic islands due to the tearing mode instability from the data of current profile evolution. They insisted that the observed disruptions are classified into three types: (1) soft major disruption caused by the overlapping of the m=2/n=1 and m=3/n=2 magnetic islands, (2) soft major disruption caused by direct contact of the m=2/n=1 magnetic island to the limiter, in which the m=3/n=2 magnetic island plays no role in the disruption process, and (3) hard major disruption which is caused by a simultaneous contact of the m=2/n=1 island with both the m=3/n=2 island and the limiter. From these observations the authors concluded that the disruption phenomena in the JIPP T-II tokamak were explained by the nonlinear saturation theory of the tearing modes and insisted that it is important to suppress the disruptions: (1) to obtain and maintain the desirable current density profile, which is attained by adjustment of both gas puffing and current ramping, and (2) to control the plasma position accurately. The second series of the disruption experiments in the JIPP T-II tokamak were carried out by Tsuji[24]. The author investigated the evolution of the magnetic islands in a detailed manner by using a tomographic imaging method of the soft X-ray signals, and concluded that an m=1/n=1 mode coupled with the dominant m=2/n=1 mode is responsible for the major disruption. The disruption scenario is rather sophisticated and roughly summarized as follows; (1) establishment of broad current profile by accumulation of impurities, (2) growth of an m=2/n=1 mode, (3) nonlinear growth of an m=3/n=2 mode, (4) occurence of a minor disruption, (5) establishment of narrow current profile, (6) growth of an m=1/n=1 mode, (7) establishment of flat current profile, (8) growth of an m=2/n=1 mode, (9) phase locking of the m=2/n=1 and m=1/n=1 modes, (10) asymmetric reconnection of the m=2/n=1 island, (11) occurence of a major disruption.

Experiments by putting emphasis on understanding the disruption phenomena were also carried out in Doublet III by JAERI team[20]. In these experiments attainment of low-q operation regime is the major objective. For the ohmic heating plasma very-low-q discharge with q less than 2 has not been realized because of the disruptions. However, the important operational conditions for achieving stable low-q (q>2) discharges are found as: (1) adequate selection of limiter material and cleanliness of the limiter and wall, (2) precise position control, and (3) slow ramping of the plasma current (<1.5 $MA\ s^{-1}$) and precisely adjusted gas puff throughput during the ramping phase of the plasma current. The remarkable feature of the disruption in this experiment is that the disruptions occur for too small and too large gas puff throughput. In the former case little radiative cooling at the edge due

to the small throughput causes a high Ni impurity influx and in the latter case the plasma edge is excessively cooled by the large throughput and both cases results in disruptions. In the NBI heating experiments very-low-q discharges with q_a as low as 1.5 have been realized[5]. In the experiment two cases with and without the NBI heating at the current ramping phase were carried out and compared each other in order to investigate the effect of current ramping on the disruptions. The reason why the disruption is suppressed during the current ramping phase with the NBI heating is not clearly understood but it may be attributed to the change of the current and temperature profiles during the NBI heating. It is important that the hard major disruptions are often observed in the very-low-q discharge with q less than 2. It seems to contradict the observation in DIVA and the disruption scenario based on the nonlinear development of the tearing modes. However, the q profile near the plasma surface is very steep and the q=2 resonant surface may lie in a scrape-off layer outside the plasma surface[5]. Therefore the mechanism of the disruption is still an open question instead of the existence of the disruptions in a very-low-q discharge.

(ii) Internal disruption

Phenomena concerning the effect of the finite beta value on the internal disruption was observed in the NBI experiments in JFT-2. As the poloidal beta value is increased the sawtooth oscillation of the soft X-ray signal changes into continuous sinusoidal oscillations (Fig.1.2.3.1)[25]. The change of the oscillational modes could be attributed to the change of the purely resistive mode to the resistive internal kink mode as shown later. In this case the boundary of the two modes is understood as the stability boundary of the internal kink mode.

1.2.3.2 Theory

(i) Major disruption

There are several theoretical models to reproduce the experimentally observed major disruptions. Among them the models based on the nonlinear tearing modes and the nonlinear kink mode are investigated minutely by numerical simulation codes. The former model relates the major disruptions in a plasma with profiles formed by edge cooling and the latter relates those in a plasma with the safety factor less than 2. The set of equations of the simulation code based on both the models is the reduced set[26] of the resistive MHD equations.

As for the nonlinear tearing mode evolution model several different cases were numerically analyzed by Azumi and Kurita. Typical one of them is the disruption scenario of nonlinear destabilization due to the overlapping islands with the m=2/n=1 and m=3/n=2 modes[27,28]. This scenario seems very plausible because the typical phenomena of the major disruption, i.e., the negative voltage spike, decrease of the plasma temperature and extinction of the equilibrium due to the destruction of the magnetic surfaces (Fig.1.2.3.2) can be explained successfully by the simulation on an edge-cooled plasma. But as seen from the variety of the experimental results this scenario cannot explain all the disruptions caused by the edge-cooling. Growth of a single helicity island with m=2/n=1 mode incorporated with transport process or the phase locking of the m=2/n=1 and m=1/n=1 islands in a toroidal geometry are attractive explanations of this kind of major disruptions. We have not, however, tried yet to find a set of parameters which causes the

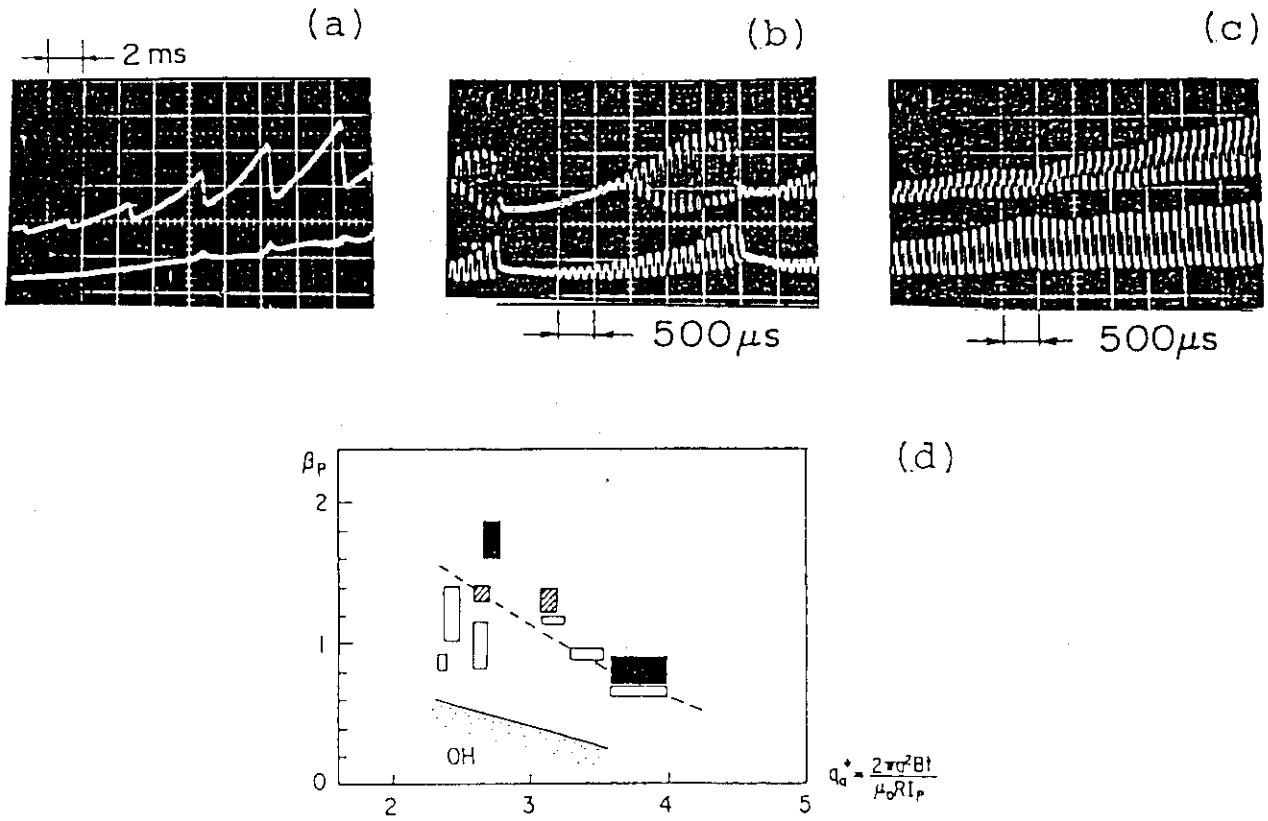

Fig.1.2.3.1 Finite beta related MHD activity observed in NBI heating experiments in JFT-2. A sawtooth oscillation of the soft X ray signal observed in a low β_p plasma (a) changes into a continuous sinusoidal oscillation (c). Subfigure (b) shows the mixed oscillation for the middle β_p plasma. These three modes are observed in different regions of the (q_a^*, β_p) diagram (d), where open, shaded, and black squares denote the sawtooth, mixed, and continuous oscillations.

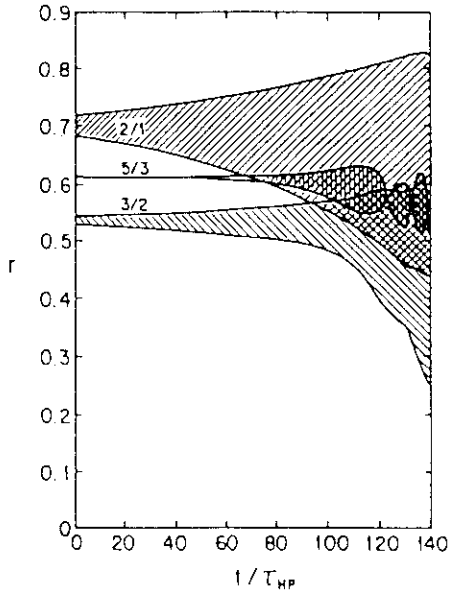

Fig.1.2.3.2(a)

Fig.1.2.3.2(b)

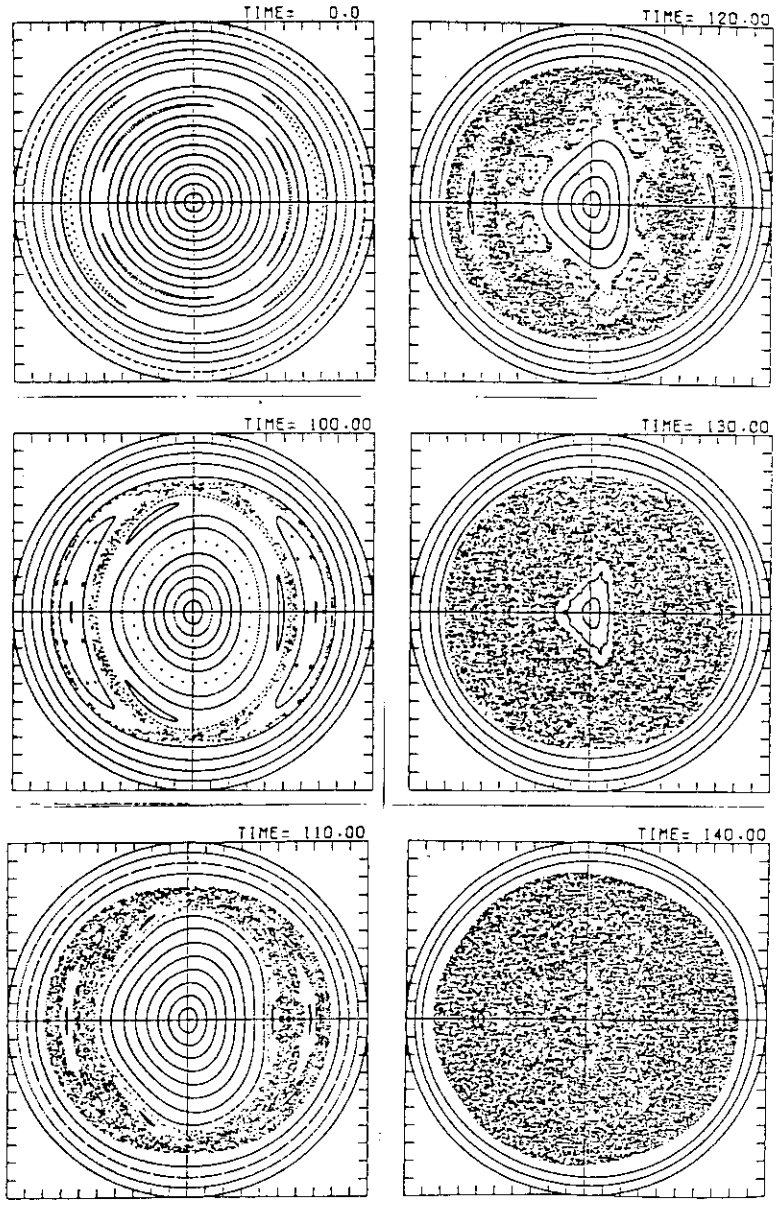

Fig.1.2.3.2 An example of the overlapping process of the magnetic islands with the m=2/n=1 and m=3/n=2 modes. (a) the time evolution of the magnetic islands, (b) the corresponding stochastization of the magnetic surfaces caused by the overlapping of the magnetic islands.

major disruptions according to these scenarios.

The mechanism of the disruptions according to the low q stability boundary was first proposed by Kadomtsev and Pogutse[29] as a magnetic bubble formation process and after that Rosenbluth et al. investigated the possibility by a numerical simulation of ideal MHD mods[30]. As they were not able to give a decisive conclusion if the process does exist in a realistic experimental situation in a resistive plasma Kurita is trying to reproduce the disruption caused by the external kink mode by a numerical simulation[31]. This simulation is based on a quasi-free-boundary technique proposed by Azumi[31] in which the vacuum region is replaced by an extremely high resistive plasma. A preliminary result obtained up to now shows that a saturated elliptical deformation and bubble formation are demonstrated for a plasma with the safety factor just below and above 2, respectively[32]. This result suggests that the disruptions may occur continuously when the safety factor cross the resonant value 2, though the underlying mechanisms of the disruptions before and after the crossing are different.

From the viewpoint of the kinetic stability analysis Itoh el al. studied the n=1 global modes comprehensively and obtained the following result[33]. The m=2 tearing mode is destabilized by the parallel current and is stabilized due to the coupling with the drift branch when beta value increases. The toroidal coupling further stabilizes the mode. The stability of the mode suggests that the occurence of the major disruption becomes infrequent if the beta value becomes high enough.

(ii) Internal disruption

In order to interpret the suppression of the internal disruption observed in a higher beta plasma stability analyses were carried out from various viewpoints. First by using the ERATO code the linear stability of the internal kink mode in high beta tokamaks is studied by Tokuda et al. for FCT equilibria with circular and elliptic cross sections and aspect ratio of 3[15,34]. (1) The stability of the internal kink mode in a circular tokamak is investigated for low-(q_s/q_0=2.5) and high-(q_s/q_0=4) shear equilibria. The results are summarized on the (q_0,β_p) plane (Fig.1.2.3.4). The unstable regions for the equilibria with q_s/q_0=2.5 and q_s/q_0=4 are surrounded by marginal stability lines and it should be remarked that there also exists the second stability region against the internal kink mode. (2) the stability of an elliptic tokamak is studied. Though the n=1 internal kink mode in a plasma with a circular cross section is marginally stable up to the first order of the inverse aspect ratio, the mode is unstable in this order when the cross section is elliptic. Therefore, an elliptic tokamak plasma is considered to be more unstable against the mode than a circular tokamak. The stability diagram of equilibria with ellipticity κ=1.2 and q_s/q_0=2.5 is presented.

Next, resistive internal kink mode is investigated as it seems important in relation with the beta effect on the internal disruption. The role of the internal kink mode in the plasma confinement is considered as follows. For low poloidal beta the azimuthal component, ξ_χ, localizes in the narrow region around the q=1 surface, whose width is much smaller than the resistive layer. For this case the unstable mode is the pure resistive one. The nonlinear development of this mode is observed as the sawtooth oscillation in a tokamak experiments. As the poloidal beta increases and the unstable internal kink mode has a large growth rate, the localization width becomes wider than the

resistive layer and this mode forms a saturated island. This situation is more likely in higher-shear and/or elliptic tokamaks. Nonlinear simulation of the mode was carried out by Tanaka et al. on the basis of a new reduced set of resistive MHD equations proposed by Azumi confirmed the phenomenon qualitatively[35] (Fig.1.3.3.5). The heating experiment in the JFT-2 tokamak shows consistent results with our theoretical analyses. It is not clarified if the resistive internal kink mode plays an important role in the beta limit or confinement degradation. Further theoretical studies based on various models are needed for the solution of the issue.

Possibility of a drift tearing mode as an explanation of the suppression of the internal disruption was also studied but extremely large number of Fourier modes were required for a complete simulation and establishment of a saturation state has not been concluded yet[31].

1.2.3.3 Comparisons and conclusions

As for the major disruptions there are various experimental findings and results of the numerical simulations. A mechanism of each disruption is not, however, identified quantitatively and at present it seems rather difficult to get from the simulation a set of quantitative data useful for designing a new devices.

Internal disruption process is well understood and rather detailed phenomena associated with the internal disruption such as the suppression of the disruption in a high beta plasma are investigated recently. As for this phenomenon the experimental and theoretical results agree each other qualitatively (Fig.1.2.3.1(d)).

1.3 R and D programs

1.3.1 On-going programs and expected advancements

1.3.2 Additional R and D needs

The limiting beta scaling seems to be established phenomenologically. But underlying mechanism of the beta limit is still unknown. It is urgently required to clarify the mechanism, which may give a guide line to attainment of an unknown higher beta state.

In a gas puffing method, high particle recycling at the periphery seems to be a key factor determining the density limit[36]. As a central fuelling method, pellet injection has been developed and demonstrated the advantage of the central fuelling to obtain a high density and well confined plasma[37,38]. Further development of pellet technology to get higher speed will be required. Experiments on large tokamaks such as JT-60 will give more relevant data in both methods. Few theoretical works on the density limit are carried out. To clarify the density limit of the tokamak plasma theoretical studies of the mechanisms and scaling law of the density limit should be accelerated.

By suppressing the disruptions we can expand the area of the operational regimes. For this purpose a well documented data base of experimentally obtained data on the disruptions and theoretical parameter survey by numerical codes based on various models are necessary.

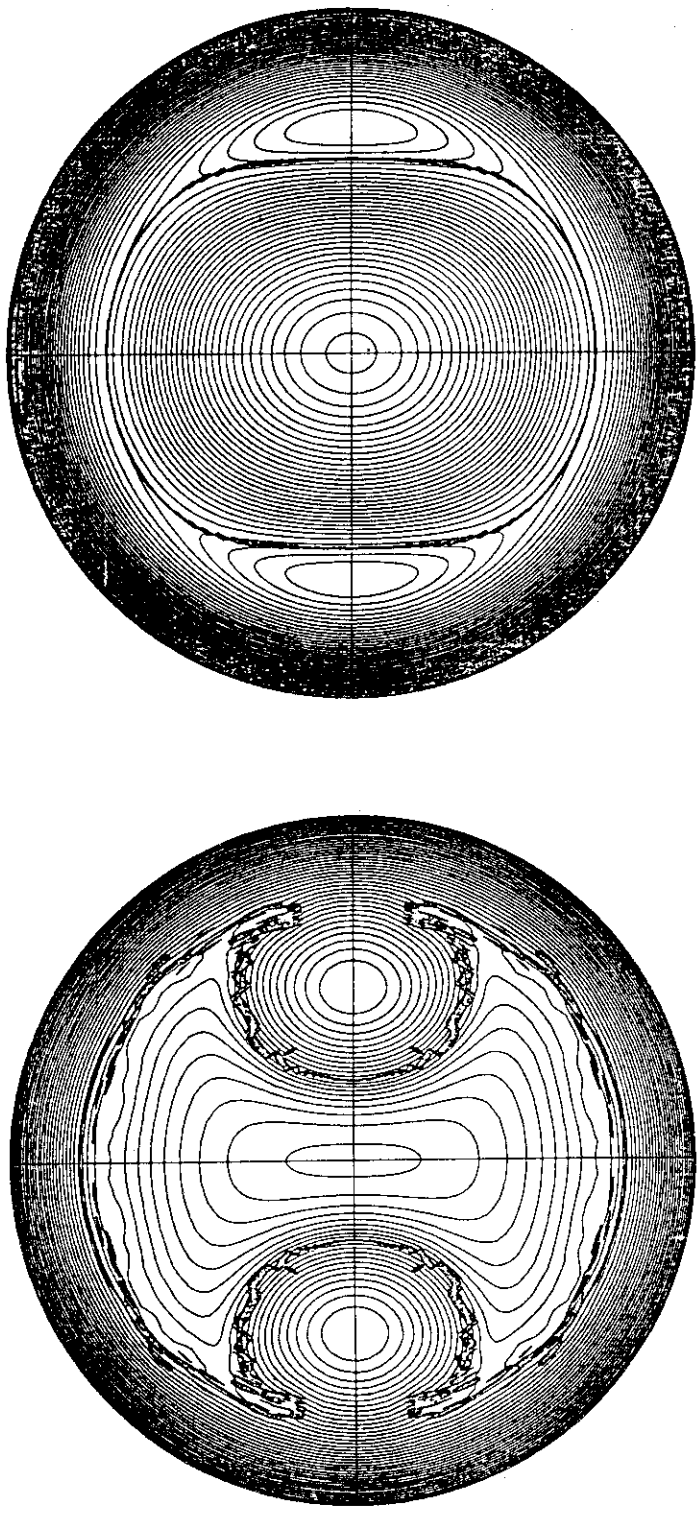

Fig.1.2.3.3 Examples of the disruption simulation due to the free boundary mode. (a) A case for the equilibrium safety factor of 2.2. (b) A case for the equilibrium safety factor of 1.9.

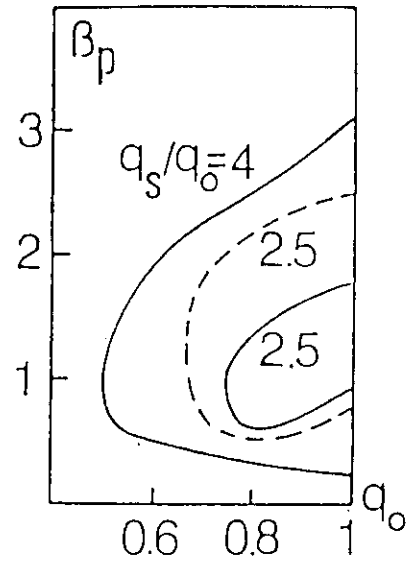

Fig.1.2.3.4 Stability diagram of the n=1 internal kink mode. Solid and broken lines denote the circular and elliptic (κ=1.2) cross sectional plasmas, respectively.

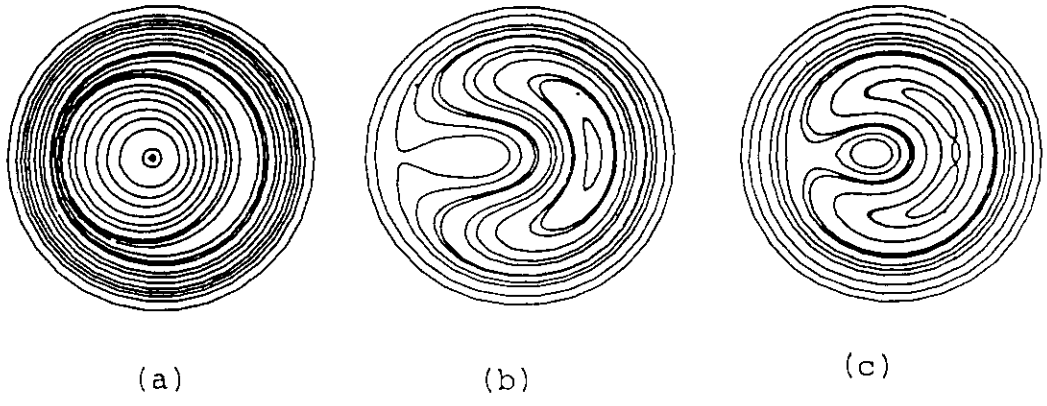

Fig.1.2.3.5 Magnetic surface configurations in a saturated states for (a) The internal mode, (b) the resistive mode, and (c) the resistive internal mode.

1.4 Impact on INTOR design

Stability analyses of the infinite-n ballooning mode and n=1 kink mode give a simple practical scaling law of $\beta_c = \hat{C}I_p$. Almost all of the experimentally obtained beta values are less than the above theoretical prediction. Therefore, it is reasonable to employ the above scaling law for designing the INTOR, though the detailed mechanism of the beta limitation is still to be investigated. According to the beta scaling law it seems very difficult to attain the aimed beta value of 5.6 % under the present design of the INTOR. The present designof the INTOR, however, does not fully make use of the information on the beta optimization of the equilibrium. There are several possibilities, e.g., increasing the triangularity by employing a double null divertor configuration, reducing the aspect ratio, and so on, to improve the INTOR from the viewpoints of the beta optimization. In any case, however, considerable changes of the INTOR design parameter seem to be necessary if the designed beta value of 5.6 % is required persistently.

In INTOR, an avrage density of 1.4×10^{20} m^{-3} is planned at B_t= 5.5T and R = 5.2 m, which corresponds to the Murakami parameter of $13\times10^{19}m^{-2}T^{-1}$. This value seems to be feasible to achieve with gas puffing method. Central fuelling with the pellet injection may be more reliable method to get over the target density.

References

1) International Tokamak Reactor - Phase IIA Part I (IAEA, Vienna, 1983).
2) K.M. McGuire, "Observation of finite-β MHD phenomena in tokamaks", Proc. 1984 International Conf. on Plasma Physics, Lausanne, 1984.
3) M. Maeno et al., Japan. J. appl. Phys. **23** (1984) 998.
4) H. Ninomiya, M. Nagami, JAERI-team, "Operational characteristics of D-shaped and circular plasmas during the neutral beam injection in Doublet III", Bulletin of the 24th American Physical Society Meeting, (Nov. 1-5, 1982) 9E8.
5) H. Ninomiya, unpublished (May, 1983).
6) A. Kitsunezaki et al., "High pressure plasma with high power NBI heating in Doublet III", in Proc. 10th International Conf. on Plasma Phys. and Controlled Nucl. Fusion Research, London, 1984, IAEA-CN-44/AI-4.
7) M. Azumi et al., "Scaling of beta limit in a tokamak for infinite-n ballooning mode", Proc. of 1984 International Conf. on Plasma Physics, Lausanne, 1984.
8) T. Tuda et al., "Accessible beta value of tokamak", in Proc. of 10th International Conf on Plasma Phys. and Controlled Nucl. Fusion Research, London, 1984, IAEA-CN-44/EIII-4.
9) L.C. Bernard et al., Nucl. Fusion **23** (1983) 1475.
10) K. Itoh et al., Nucl. Fusion **22** (1982) 1031
11) S. Tokuda et al., "MHD stability analysis by revised version of ERATO-J", JAERI-M 9899 (1982).
12) M. Azumi et al.,"Evolution of stable high-beta tokamak equilibria", Plasma Physics and Controlled Nuclear Fusion Research, 1980, (IAEA, Vienna, 1981) Vol.1p.293.
13) A. Sykes et al., "Beta limits in tokamaks due to high-n ballooning modes", Proceedings of the 11th European Conference on Controlled Fusion and Plasma Physics, (1983) Vol 2, p.363.
14) F. Troyon et al., Plasma Phys. **26** (1984) 209.
15) T. Takeda et al., "Physics of intensely heated tokamak plasma", in Plasma Physics and Controlled Nuclear Fusion Research 1982, (IAEA, Vienna, 1983) Vol.3, p.23.
16) T. Tsunematsu et al., "MHD equilibrium and stability of anisotropic pressure plasma", unpublished report (1984).
17) DIVA group, Nucl. Fusion 20 (1980) 271.
18) N. Suzuki et al., in Plasma Physics and Controlled Nuclear Fusion Research (Proc. 8th International Conf., Brussels, 1980), (IAEA, Vienna, 1980) Vol.2, p.525.
19) T. Shoji et al., in Controlled Fusion and Plasma Physics (Proc. 11th European Conf., Aachen, 1983) Vol.1 (1983) p.55.
20) M. Nagami et al., Nucl. Fusion 22 (1982) 409.
21) M. Murakami et al., Nucl. Fusion **16** (1976) 347.
22) M. Maeno et al., J. Phys. Soc. J. 48 (1980) 273.
23) K. Toi et al., Nucl. Fusion 22 (1982) 465.
24) S. Tsuji, "Soft X-ray imaging study on disruptions in the JIPP T-II tokamak", IPPJ-630 (1983).
25) S. Yamamoto et al., "Transport studies in the JFT-2 tokamak", in Plasma Physics and Controlled Nuclear Fusion Research 1982, (IAEA, Vienna, 1983) Vol.1, p.73.
26) B.V. Waddell et al.,Nucl. Fusion **16** (1976) 528.

27) B.V. Waddell et al., Phys. Fluids **22** (1979) 896.
28) G. Kurita et al., "Major Disruption Process in Tokamak", JAERI-M 9788 (Nov. 1981).
29) B.B. Kadomtsev, O.P. Pogutse, Sov. Phys. JETP 38 (1974) 283.
30) M.N. Rosenbluth et al., Phys. Fluids 19 (1976) 1987.
31) T. Tsunematsu et al., "Nonlinear evolution of external kink mode in tokamak and comment on resistive internal kink mode", in Proc. of US-Japan Workshop on 3D MHD Studies, 1984, Oak Ridge, CONF-840370, p.158.
32) G. Kurita, private communications (Oct, 1984).
33) K. Itoh et al., J. Phys. Soc. Japan **53** (1984) 1759.
34) S. Tokuda et al., Nucl. Fusion **22** (1982) 661.
35) M. Azumi et al.,"Internal disruption in high β_p tokamak", JAERI-M 9787 (Nov., 1981).
36) N. Ohyabu, Nucl. Fusion **19** (1979) 1491.
37) M. Greenwald et al., Phys. Rev. Letters **53** (1984) 352.
38) S. Sengoku et al., in Proc. 10th International Conf. on Plasma Phys. and Controlled Nucl. Fusion Resarch, London, 1984, Post Deadline Papaer.

2. Confinement

2.1 Physics design assumption and parameter (Phase IIA)

INTOR plasmas have their parameters with 5.3 m and 1.2 m of major and minor radii, 1.6 of plasma elongation, 10 keV of average ion temperatures, 1.4×10^{20} m^{-3} of average ion densities, 6.4 MA of plasma currents, 5.4 T of toroidal field, 124 MW of alpha heating power. Those parameters were originally based on the INTOR(ALCATOR) scaling. Confinement potential of INTOR also strongly depends on the scalings of confinement time, which widely spread at present from favourable to unfavourable scalings. Particle confinement performance is also crucial for helium exhaust, and cool and dense divertor operation capability. Helium concentration in a main plasma is considered to be 5 %, and the cool and dense divertor plasmas needs considerably high particle flux into the divertor region of the order of 10^{22} /s. Such a particle confinement potential also hinges on the scalings of particle confinement time.

2.2 Data base

2.2.1 Energy confinement

(a) Ohmically heated plasma

Energy confinement properties of ohmically heated plasmas in Doublet III were compared for D-shaped and circular cross section plasmas with an identical minor radius as functions of plasma current, electron density, and vertical elongation under a wide range of discharge conditions [1].

Figure 2.1 shows the relation ($\tau_{Ee}\langle I_p\rangle/(B_T[1+K(a/2)^2]/2)\propto \tau_{Ee}/q^*$) of the electron energy confinement time τ_{Ee} versus $\langle n_e\rangle$ in the wide range of plasma parameters shown in the figure, where 1.5 times neoclassical is used as the ion energy confinement. $\langle I_p\rangle$ is the plasma current inside r=a/2. The ellipticity K(a/2) is 1.0, 1.2, 1.4 for discharges with K(a)=1.0, 1.4, 1.7, respectively. Here, the dependence of τ_{Ee} on q* in the present expression is similar to but slightly stronger than the dependence of τ_E on q_a* observed in DIVA ($\tau_E\propto\bar{n}_e\sqrt{q_a^*}$) [2], and JFT-2 [3].

The vertical elongation of the plasma cross section and the plasma current are related to each other in the behavior of gross energy confinement τ_{EeG}, where $\tau_{EeG}=\int 3/2n_eT_edV/I_pV_l$, and for $T_e=T_i$, τ_{EeG} is equal to $\tau_E/2$ (Fig. 2.2). The dependence of the gross energy confinement time on the elongation and the plasma current is different in different electron density regions. This behavior of the gross energy confinement can be explained by the combination of the electron energy confinement τ_{Ee} proportional to $\bar{n}_eq^*(\propto(\bar{n}_eB_T/I_p)(1+K^2)/2)$ and the neoclassical ion energy confinement τ_{Ei} proportional to $I_p^2/\bar{n}_e$ [1], or by the combination of the low density Ohmic scaling ($\tau_{E,OH}\sim\bar{n}_e\sqrt{q}$) and the L-mode scaling of beam-heated plasmas ($\tau_{E,AUX}I_p^2/\langle\bar{n}_eT\rangle$) [12]. The high current operational capability of D-shaped plasmas produces a remarkable improvement in energy confinement in high density plasma regions, because of the reduction in the heat loss due to τ_E or $\tau_{E,AUX}$. The highest τ_E (75 msec) is obtained for high current D-shaped discharges.

In the low density regime, the gross energy confinement times of

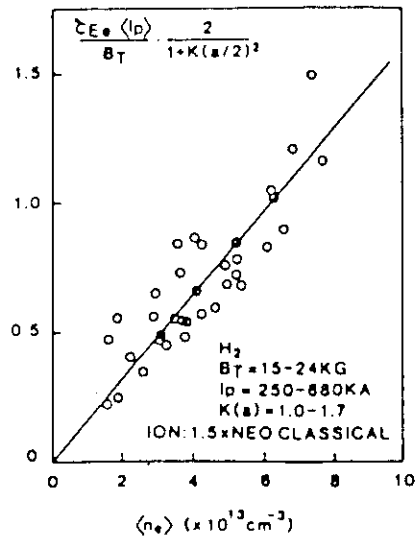

Fig. 2.1 $\tau_{Ee} < I_p > / (B_T(1+K(a/2)^2)/2)$ versus $< n_e >$. τ_{Ee} is proportional to $< n_e > q^*$.

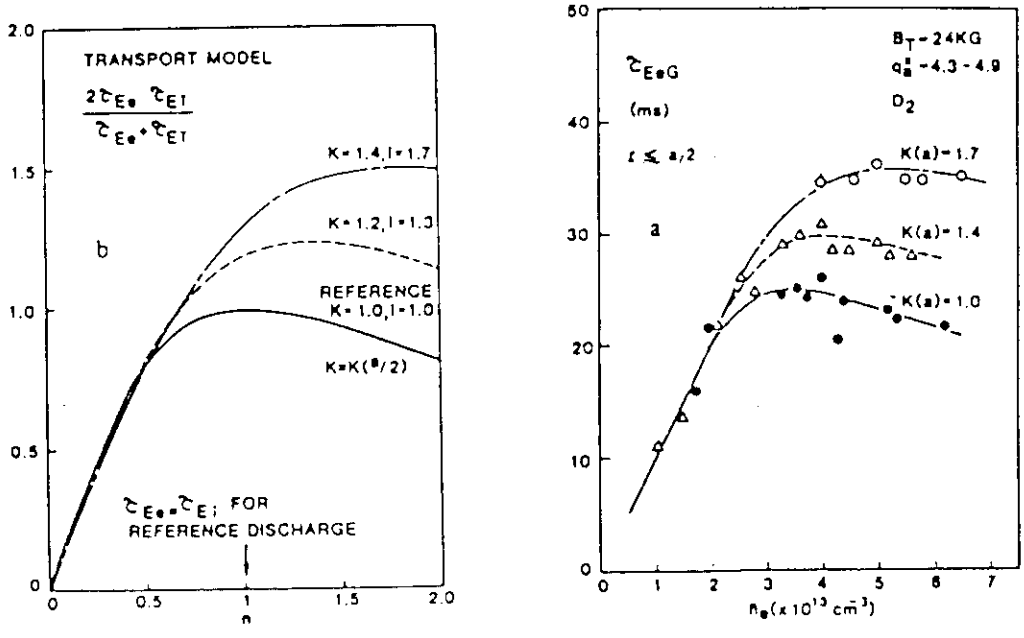

Fig. 2.2 (a) Comparison of τ_{EeG} for discharges of K(a)=1.0, 1.4, and 1.7 with constant q_a^*. In the high-density region, τ_{EeG} is improved by 65% with the vertical elongation from K(a)=1.0 to 1.7; (b) transport model calculation based on Eqs.(2) and (3). n and I are non-dimensional electron density and plasma current.

Ohmically heated plasma in DIVA, JFT-2, Doublet III, JFT-2M [4] and JIPP-T II [5] are almost same with that expected by neo-Alcator scaling ($\tau_E=0.19\times10^{-20}\bar{n}R^2a$) as shown in Fig. 2.3. If we use the medium q-scaling ($\tau_E\sim q^{3/4}$) from results of DIVA ($\tau_E\sim\sqrt{q}$) and Doublet III ($\tau_E\sim q$), neo-Alcator scaling is changed to the following form; $\tau_E=10^{-21}q^{3/4}\bar{n}R^2a$. A centrifuge pellet injector was employed to produce and maintain high density peaked profiles with low edge recycling in the Doublet III tokamak [13].

In gas fueled divertor ohmic discharges, the recycling and the neutral pressure both at the edge and the divertor region, increase nonlinearly as the density is raised above 4×10^{13} cm^{-3}. The energy confinement time saturates near 60 ms (Fig. 2.4). In contrast to that, the pellet fueled confinement times continue to improve with increased density. This is probably due to the fact that in the pellet fueled discharges both the edge pressure and the limiter recycling light are maintained at relatively low levels (Fig. 2.4) and/or the successful density rise at the plasma center which has good confinement properties. The "stairstep" increase of $\bar{n}_e$ is also observed in the divertor configuration.

(b) Neutral-beam heated plasma

The neutral-beam heating experiments in Doublet III [6], JFT-2 [7], and JFT-2M showed degradation (L-mode) of confinement in comparison to the ohmic heating case, as shown in Fig. 2.5. Recently, H-mode discharges have also been observed in divertor operation in Doublet III as well as in ASDEX.

The observation of the recycling particle flux intensity at the main plasma edge for various limiter and divertor discharges indicates that the gross energy confinement of beam-heated discharges is closely related to the intensity of the edge particle flux. In limiter discharges, the global particle confinement time and the energy confinement time show many similarities: 1) linear I_p dependence for $I_p<600$ kA; 2) no B_T dependence; and 3) deterioration as a function of the injection power. Improvement of τ_E by increasing I_p, for example, is associated with high temperatures in the plasma edge region accompanied by reduced particle recycling (Figs. 2.5.(a), 2.6).

The divertor equilibria allow a wide variety of edge recycling, depending on gas puff intensity, rotational transform of scrape-off field line, plasma current, etc. Divertor discharges with low particle recycling around the main plasma show better energy confinement than limiter discharges at high plasma densities. The energy confinement time of these discharges is proportional to n_e (scales as INTOR scaling). The improvement in τ_E stems primarily from the reduction of heat transport in the main plasma edge region, which is associated with the reduction of the recycling particle flux at the main plasma edge. In certain conditions of operation, e.g. excessive cold gas puffing, the discharge shows a relatively high scrape-off plasma density and strong particle recycling between main plasma and limiter. The energy confinement time of these discharges is somewhat degraded, compared to INTOR scaling, or even reduces completely to that of the limiter discharge.

In low-recycling divertor discharges, the central electron and ion temperatures are proportional to the injection power, and the stored plasma energy is proportional to n_eP_{abs} (Fig. 2.7). With about 4 MW beam injection, high temperature and high density plasmas were obtained (stored energy up to 280 kJ, $T_e(0)=T_i(0)=2.5$-3.0 keV at $n_e=(6$-$7)\times10^{13}$ cm^{-3}, $\tau_E=70$ msec).

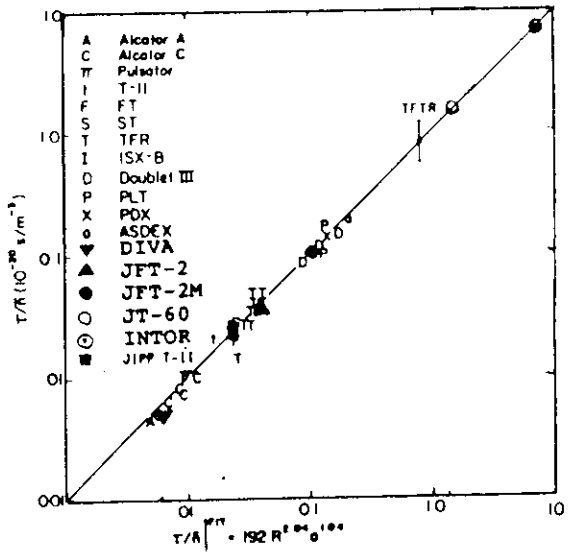

Fig. 2.3 Regression fit to data from low Z_{eff}, low P_{rad}, moderate q, confinement experiments, from Alcator C group.

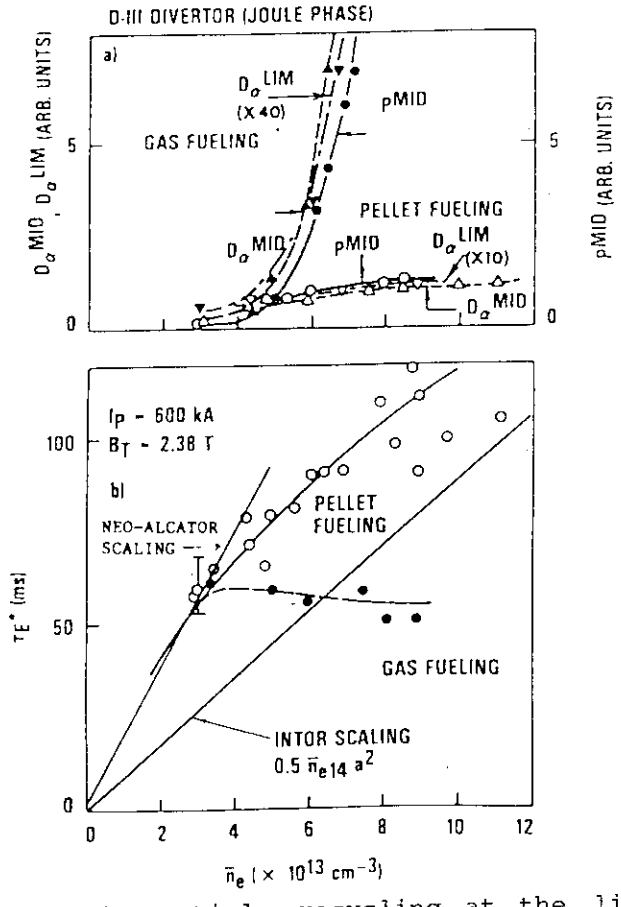

Fig. 2.4 Comparison of a) particle recycling at the limiter and divertor region as inferred from D_α LIM and D_α MID and the neutral pressure at the divertor region and b) the energy confinement time between gas and pellet fueled discharges as functions of $\bar{n}_e$. Open symbols denote pellet fueled discharges; and solid symbols, gas fueled discharges.

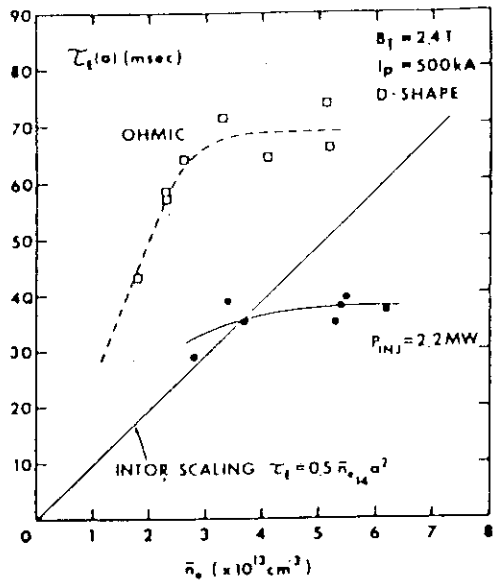

Fig. 2.5 (a) Density scaling experiments by JAERI D-III team. D target, L-mode.

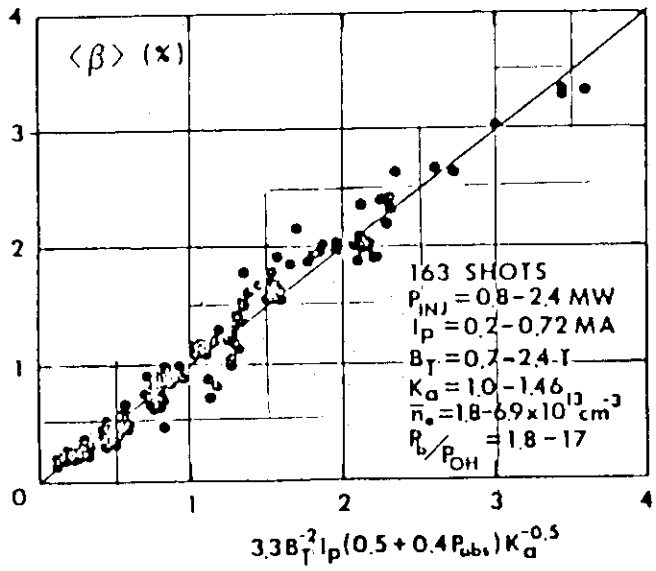

Fig. 2.5 (b) Under a wide parameter range, $\langle\beta\rangle$ scales as $\beta\,[\%] = 3.3 B_T[T]^{-2} I_p[MA]\,(0.5 + 0.4 P_{abs}[MW]) K_a^{-0.5}$.

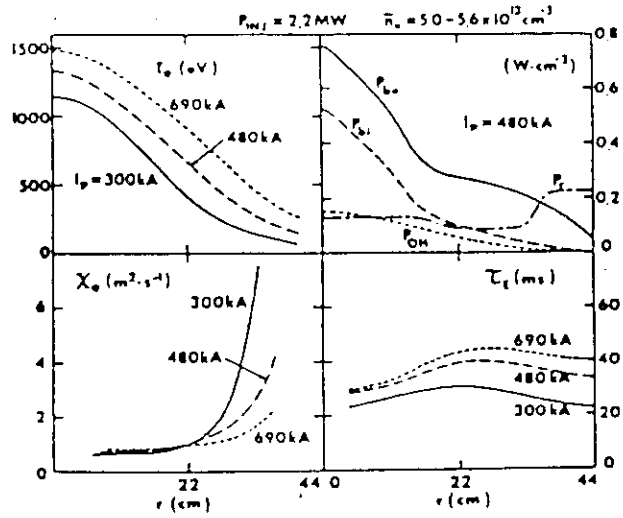

Fig. 2.6 Comparison of energy transport for three discharges with different I_p. T_e, P_{be}, P_{bi}, P_{OH}, P_r, χ_e, and τ_E are shown versus r. For simplicity, we neglect the convective heat flux in the present calculation.

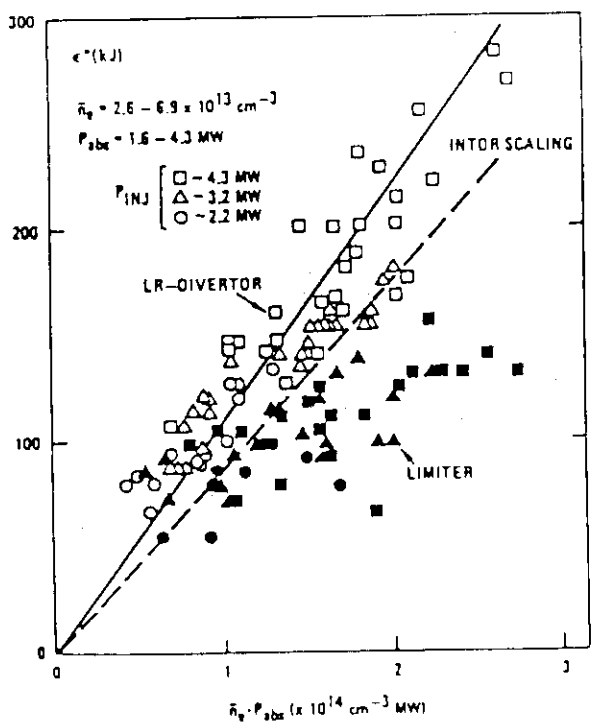

Fig. 2.7 Stored plasma energy $\in^*$ versus $\bar{n}_e P_{abs}$ for LR-divertor and limiter discharges.

Especially with high power injection, the D-D thermonuclear fusion neutron yield of the LR-divertor is larger than that of a limiter discharge by a factor of as much as about eight. This suggests the importance of edge particle recycling control, in particular, for the thermonuclear breakeven demonstration in the next generation tokamaks.

A high plasma current is important to realize high $\bar{n}_e$ and low recycling divertor discharges; it results in high $\bar{n}_e \tau_E$. This is due to the better particle confinement for higher I_p and the short connection length between the main plasma and the divertor plate along the scrape-off field line, because of lower q.

The present experiments indicate that, to realize a low particle recycling state around the main plasma, it is important to prevent the backflow of neutral gas produced in the divertor region. In this sense, a closed divertor configuration is more favourable than an open divertor geometry. In the (mechanically) closed divertor configuration, however, there may be a high density (best τ_E) limit, which is probably determined by the break of the low recycling state due to the formation of large particle recycling near the narrow divertor throat, when the divertor scrape-off plasma becomes too dense. Optimization of the divertor equilibria and divertor throat width for closed divertor geometry and application of the results of Doublet III open divertor geometry are important tasks to be embarked upon in the future.

Recently, the experimental results with high plasma current (1 MA) and high power (8 MW) NBI heating with hydrogen and deuterium beam were reported [14]. The central ion and electron temperature of H-mode discharge increase almost linearly to the absorbed power up to $\sim$7MW and attains more than 5 keV as shown in Fig. 2.8. The amount of energy stored in the plasma measured by the diamagnetic loop increases almost linearly with the increase of absorbed power as shown in Fig. 2.9. The volume averaged beam component of high NB heating is estimated to be 10-20 % (at $\bar{n}_e$=7-4x10^{13} cm^{-3}). The stored energy of a limitered discharges is still on the scaling $W_{st}=c(0.5+0.4P_{abs})$ as we reported before for NBI power of < 2 MW [6].

The neutron production rate with a deuterium beam injection into a deuterium plasma reached 1.0x10^{15} neutron/sec. Hydrogen beam injection into hydrogen plasma with 4-5 MW was also attempted, but no H-mode was observed. The global energy confinement time is shown in Fig. 2.10 as a function of plasma density. As shown in the figure, there is no data at low plasma density with high confinement time.

The improvement of energy and particvle confinement in pellet produced plasmas has been established in both ohmic and beam-heated limiter and divertor discharges. The energy confinement is seen to improve with increasing density, in contrast to the saturation found in gas fueled plasmas [13].

While the confinement of pellet-produced beam heated plasmas deteriorates with time and with increasing beam power, a method of interrupting the beams has produced sustained high confinement discharges with suppressing pellet edge ablation. The enhancement of the ablation at the edge by neutral beam is found to be responsible for the confinement deterioration. A simple model calculation shows that the lower energy components of the beam

particles which are supposed to deposit at the edge may be important for the edge ablation. The reduction of edge density and recycling seems to be a key aspect of the improved confinement along with the peaked central densities.

Since the pellet-produced low recycling divertor discharges contradict the merit of "dense and cold divertor [15]", the independent control of divertor plasmas might be important for pellet injection in divertor configurations. The combination of the improved confinement and the high densities has produced a significant extention of the $\bar{n}_e$, τ_E* diagram (Fig. 7) for D-III. The Lowson product $\bar{n}_e(0)\ \tau_E$* is increased by a factor of 3 to 4 in both limiter and divertor discharges. The neutron production rate has been improved by a factor of 10 over limiter beam-heated plasmas of comparable gas fuelled discharges. These results are very encouraging for large nondivertor tokamaks that will rely heavily on neutral beam heating to produce energy breakeven conditions.

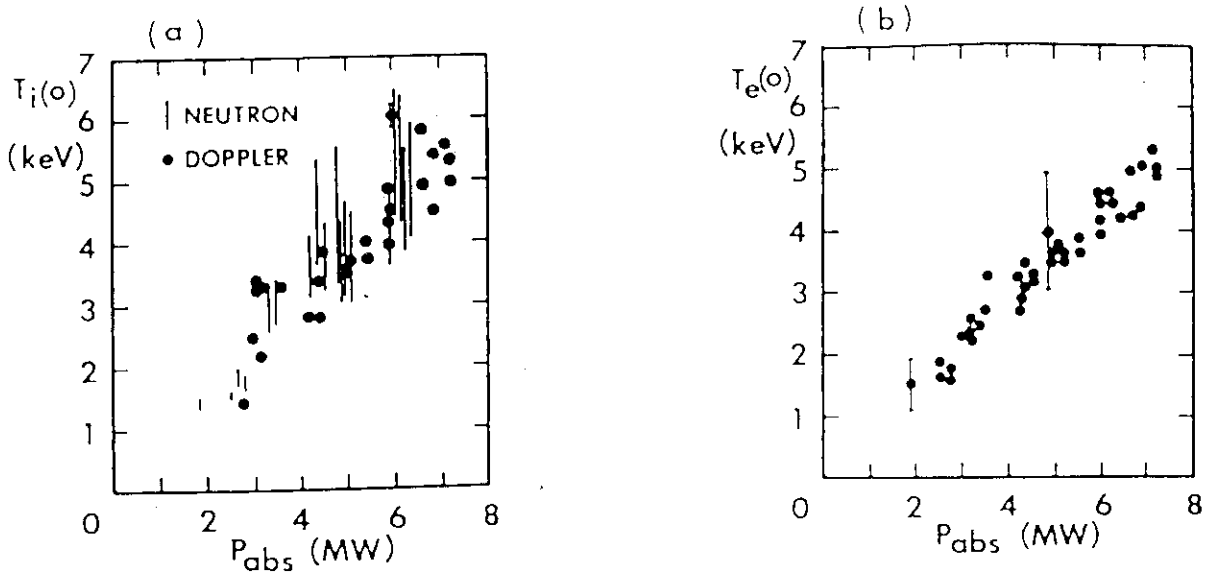

Fig. 2.8 Central ion temperature (a) and electron temperature (b) vs. absorbed power. The ion temperature by neutron has an ambiguity due to uncertainty of hydrogen (beam species) population. The electron temperature at $T_e > 4.5$ keV is measured by the grating $2\omega_{ce}$ radiometer. $\bar{n}_e$=4-7.5x10^{13} cm^{-3}, I_p=750-800 kA. B_T=2.0-2.6 T.

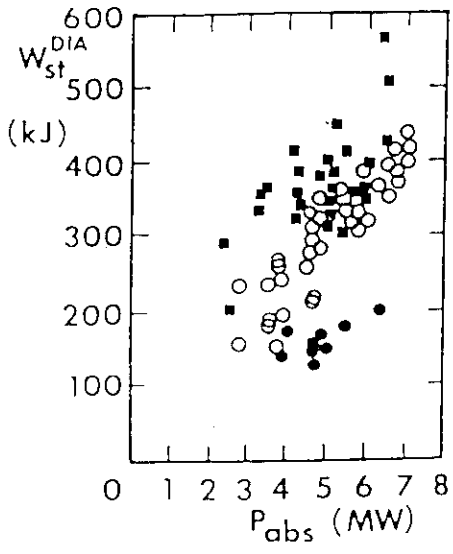

Fig. 2.9 Stored energy vs. absorbed power. (■) H-mode divertor discharge, D beam injection to D plasma, (○) H-mode divertor discharge, H beam to D plasma, (●) Limitered discharge, H beam to D plasma. I_p=800-900 kA (divertor), 740-800 kA (limiter), B_T=2.0-2.6 T.

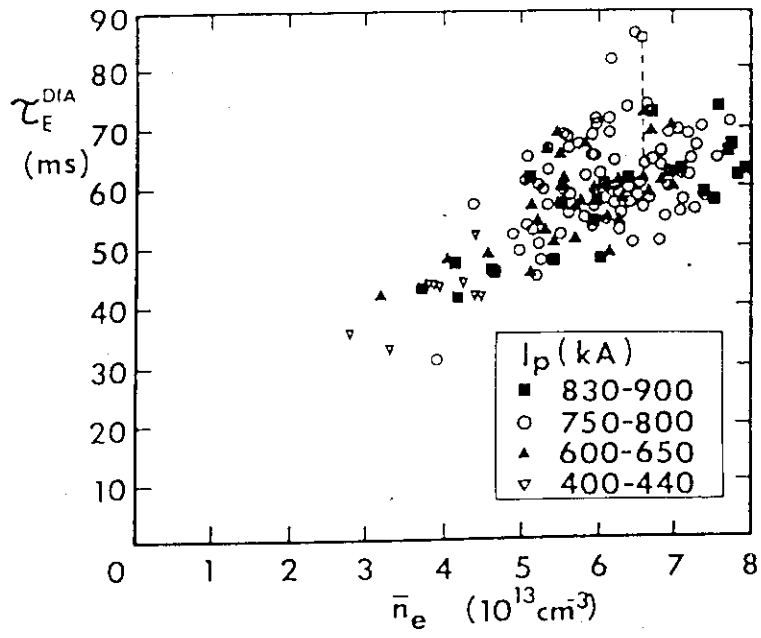

Fig. 2.10 Global energy confinement time. The confinement time of good divertor discharges increases as plasma density increases. B_T=2.0-2.6 T, hydrogen beam injection into diverted deuterium plasma. The energy confinement time during β_p increase is shown by for one case.

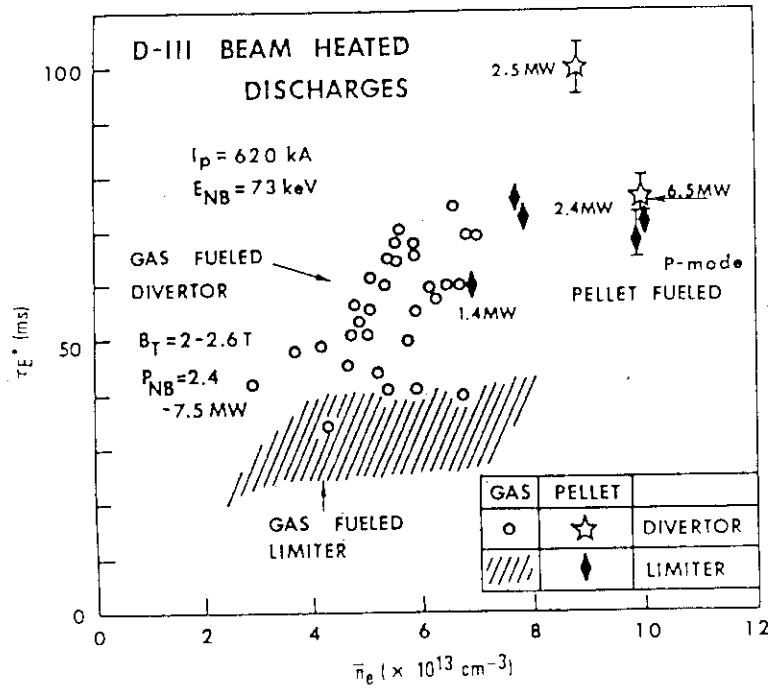

Fig. 2.11 Comparison of $\bar{n}_e$, τ_E* plot between pellet and gas fueled discharges for both limiter and divertor configurations with continuous beams. The upper envelope of open circles corresponds to D-III H-mode discharges. For gas fueled discharges, τ_E* is calculated when dW/dt=0.

(c) RF-heated plasma

(ICRF)

ICRF heating experiments in DIVA [9a] showed a very slightly degradation of confinement time (Table 1) that was obtained by measurements of the e-folding decay time of bulk ion temperature after the termination of rf pulse and assuming that the rf power to electrons was negligeble. Experiments [9b] in JFT-2 showed that the rates of deposited power to the launched power obtained by assuming that the transport properties of the ohmic plasma did not change during rf heating, were as follows; 1) 60-70 % for both case of n_H/n_D=2-4 % and 10 %, 2) 80-90 % for n_H/n_D=30 % case. Therefore, the degradation of the confinement time are below 1) 30-40 % and 2) 10-20 %.

Recently, high power ICRF heating experiment has been performed in two-ion-hybrid heating regime in JFT-2M [16].

The density dependence of the gross energy confinement time is shown in Fig. 2.12. The gross energy confinement time and the total input power are defined by $\tau_{EG}=W/P_{tot}$ and $P_{tot}=P_{RF}+P_{OH}$, where W is the stored energy of the plasma. In Ohmic heating, τ_{EG} has a linear dependence on the line averaged electron density when the electron density is lower than 2.5×10^{13} cm^{-3}. There is also the same tendency in the case of ICRF heating. Thus, the density dependence of the gross energy confinement time can be represented by $\bar{n}_e(1-0.083\bar{n}_e)$ with $\bar{n}_e$ in 10^{13} cm^{-3}, approximately.

The power dependence of the stored energy is shown in Fig. 2.13. In order to eliminate the density dependence of confinement, we define W* by $W^*=W/[\bar{n}_e(1-0.083\bar{n}_e)]$. The figure indicates the degradation of τ_{EG} in the ICRF heating, but the degradation is not so large in this case as in the NBI heating case. We can not conclude that the deterioration of the energy transport or the radiation cooling by the impurities causes the degradation of τ_{EG}. Because there is a possibility that a part of the rf power is absorbed in the peripheral region of the plasma. There is not a difference between I_p=164 kA and I_p = 228 kA within the experimental accuracy. The I_p dependence of the gross energy confinement time as seen in NBI heating experiments can not be observed in our two-ion-hybrid ICRF heating experiments and Ohmic heating experiments.

TABLE I. POWER BALANCES WITH AND WITHOUT RF POWER
$P_{OH} \cong 85$ kW, $P_{Net} \cong 100$ kW, $\epsilon_p = 5-10\%$, $B_T = 18$ kG

W_e	W_i	Q_{ei}	τ_{Ee}	τ_{Ei}					Without RF
141 J	95 J	20 kW	2.2 ms	4.8 ms					
W'_e	W'_i	Q'_{ei}	τ'_{Ee}	τ'_{Ei}	Q^e_{RF}	Q^i_{RF}	η_e	η_i	With RF
158 J	151 J	3 kW	$\lesssim$ 1.9 ms	3.7 ms	?	38 kW	?	~ 40%	

Figure 2.14 shows the ICRF heated discharge in JIPP-T IIU [17]. The ion cyclotron resonance layer is located at about a half of plasma radius, and the hybrid resonance layer exsists in a central plasma region. The central electrton temperature quickly increases to about 2.0 keV after about 5 ms and slowly decreases with a large sawteeth modulation, while a central deuteron temperature (T_{Do}) increases slowly with a rise time of about 20 ms, consistent with the D-D neutron emissions. The value of S ($= \beta_p + l_i/2$) from a magnetic measurement appreciably increases although the plasma current is increased. Values of l_i and β_{pe} (electron component) are estimated from a magnetic diffusion equation using the observed T_e(Fig. 2.14(b)) and n_e profiles. The stored energy estimated from β_p ($=S-l_i/2$), β_{pe}, and β_{pi} ($= \beta_p - \beta_{pe}$) continuously increases during rf pulse. We also show the time evolutions of the stored energy (W_p, W_{pe} and W_{pi}), ohmic input (P_{OH}) and global energy confinement time ($\tau_{EG}=W_p/(P_{OH}+P_{rf}-W_p)$). The confinement time τ_{EG} increases with $\bar{n}_e$, and approaches to the value expected from the ohmic scaling in the quasi-steady state. The increase in W_{pe} in time is caused by the broadening of T_e profile and increase in $\bar{n}_e$ rather than a significant heating at the center. In Fig. 2.14(c), we show ΔW_p, $n_e \Delta T_{eo}$ and $n_e \Delta T_{Do}$ as functions of P_{rf}, while $\bar{n}_e \Delta T_{eo}$ and $\bar{n}_e \Delta T_{Do}$ do not exhibit a linear dependence of P_{rf}. This suggests the radial profiles become broad with the increase in P_{rf} asisted by GP and CR.

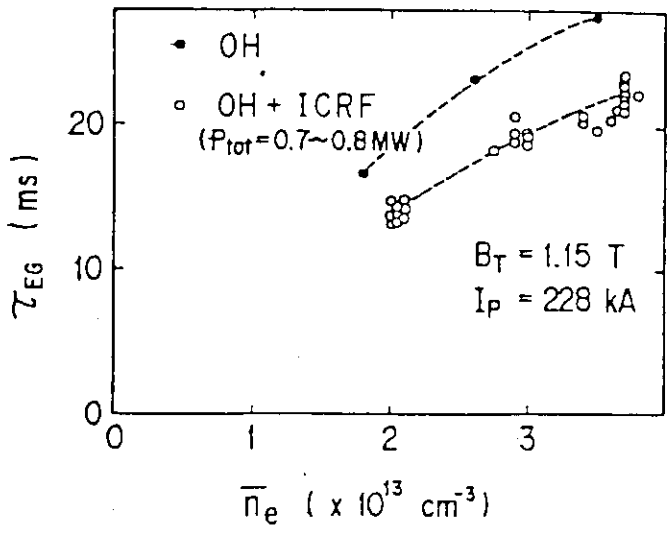

Fig. 2.12

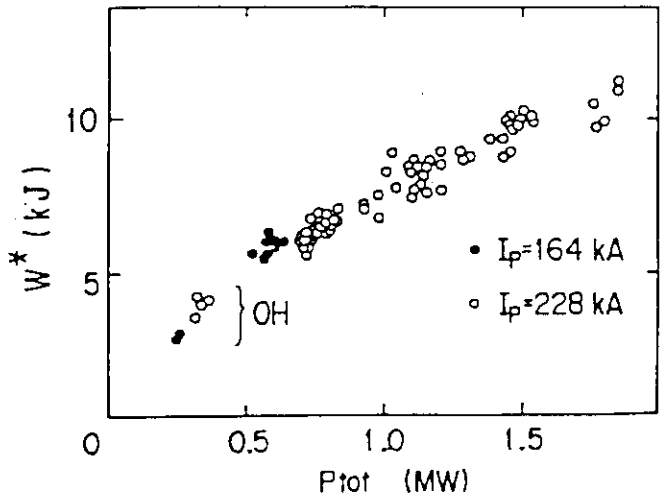

Fig. 2.12-13 The density dependence of the gross energy confinement time $\tau_{EG}=W/P_{tot}$ is shown in Fig. 2.12 where W is the stored energy of the plasma and P_{tot} is the total input power of the Ohmic heating power and the net input power of the ICRF. The density dependence of τ_{EG} can be represented approximately by $\bar{n}_{e13}(1-0.083\bar{n}_{e13})$ with $\bar{n}_{e13}$ in 10^{13} cm^{-3}. The power dependence of the normalized stored energy $W^*=W/[\bar{n}_{e13}(1-0.083\bar{n}_{e13})]$ is shown in Fig. 2.13 in the cases of I_p=228 kA and I_p=164 kA.

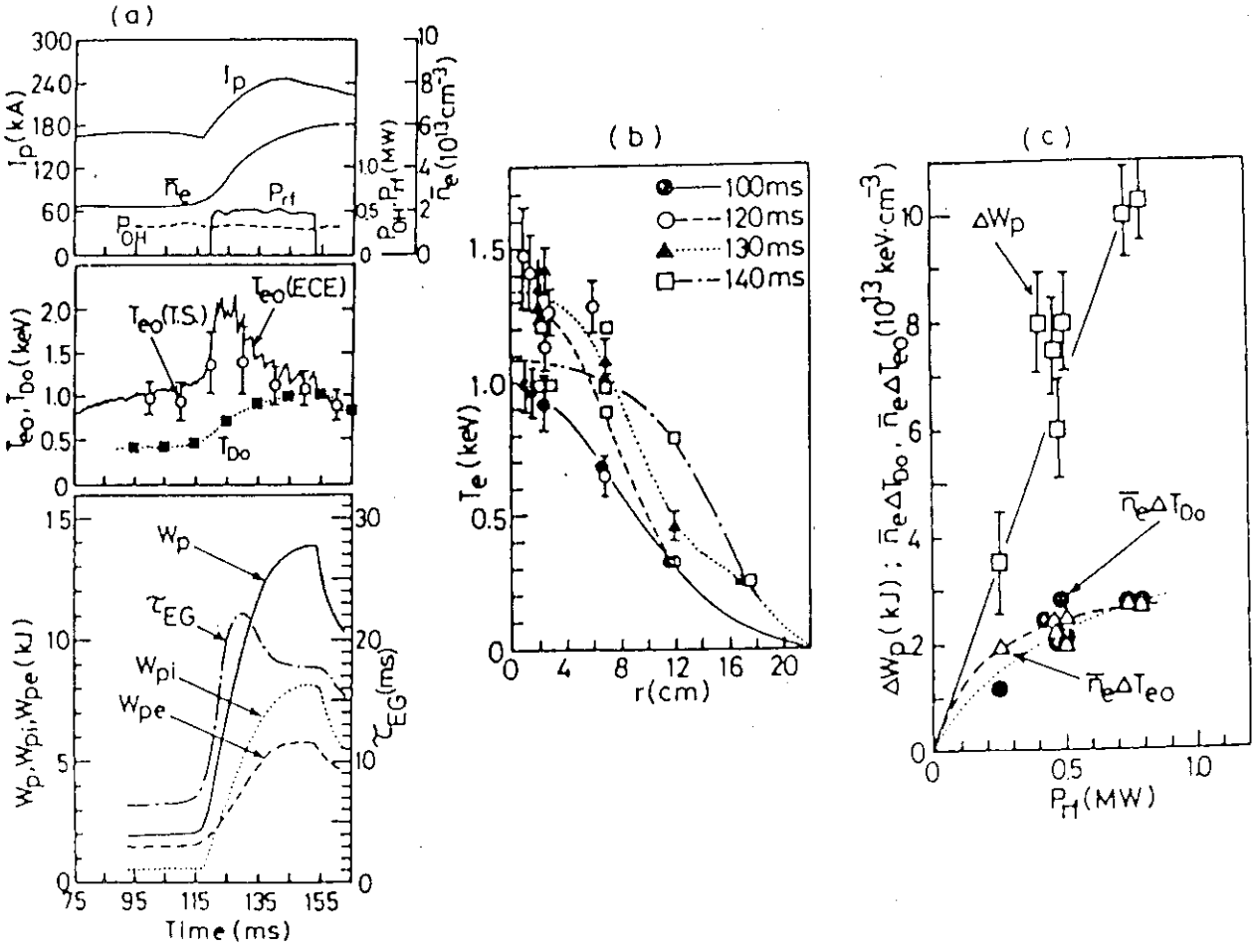

Fig. 2.14 (a) Discharge waveforms in case B. (b) Time evolution of electron temperature profile. (c) Dependence of various stored energies on P_{rf}.

(ECRH)

Overall electron energy confinement time τ_{Ee} is obtained from a simple power balance equation and expressed as

$$Ee = \frac{W_e}{P_j + P_{e,rf} - P_{ei}} .$$

Here, W_e denotes plasma energy of electrons $P_{e,rf}$ deposited rf power to the electrtons and P_{ei} power to the ions from electrons. $P_{e,rf}$ is written as $P_{e,rf} = P_{rf}$ where P_{rf} is a net rf power. We take η as 100 %, which gives the lowest estimation of the energy confinement time. The calculated confinement time of Joule plasmas $\tau_{Ee,j}$ and that during rf $\tau_{Ee,rf}$ is given in Table 2(a), (b). The energy confinement time during rf is not worse than that of the joule plasma.

τ_{Ee} is also obtained from rise time or fall time of the electrton temperature. The result was 4-5 msec for during rf. Thus there is a good agreement in τ_{Ee} from these estimations [10].

Table 2 Electron energy confinement time, (a) without rf, (b) with rf.

(a)

$n_e(0)$ ($10^{12}cm^{-3}$)	$T_e(0)$ (eV)	V_L (V)	I_p (kA)	P_j (kW)	τ_{ei} (msec)	P_{ei} (kW)	W (J)	$\tau_{Ee,j}$ (msec)
5	700	1.4	75	105	42	3.2	190	1.9
10	600	1.4	75	105	17	13	320	3.5
15	500	1.5	75	113	8	30	400	4.8
20	500	1.5	75	113	6	53	530	8.8

(b)

$n_e(0)$ ($10^{12}cm^{-3}$)	$T_e(0)$ (eV)	ν_T	ν_n	$V_{L,rf}$ (V)	I_p (kA)	P_j (kW)	τ_{ei} (ms)	P_{ei} (kW)	W (J)	P_{rf} (kW)	$\tau_{Ee,rf}$ (ms)
12	240	3.5	2.0	1.1	75	80	41	12	610	85	4.0

2.2.2 Particle confinement

(D-III)

Figure 2.9 shows τ_p versus the plasma current for ohmically and beam-heated discharges. Since τ_p depends strongly on n_e in limiter discharges, we studied τ_p versus I_p at constant $\bar{n}_e(=(4-5)\times10^{13}\ cm^{-3})$. The fiture shows that τ_p decreases with beam injection: 18-24 msec (Ohmic) to 7-18 msec (NBI). This means that edge particle recycling is enhanced with beam injection by a factor of 1.4-2.8 with respect to the ohmic heating level. The important feature is that τ_p is proportional to I_p for beam-heated plasmas. This is consistent with the observation that the density clamps with beam injection into limiter discharges, i.e. the density clamping is stronger for smaller plasma currents of $I_p < 500$ kA [6].

(JFT-2)

Time τ_p and the trapping efficiency were measured in various conditions. The results of particle confinement measurments are shown in Fig. 2.10. Here, we have assumed that $\tau_p = \sqrt{q_a}\bar{n}_e$, which was confirmed in the DIVA tokamak; τ_p is plotted against $\sqrt{q_a}\bar{n}_e$ From this relationship, it is shown that, with injection, τ_p levels off slightly as compared with the Ohmic heating case. The maximum reduction of τ_p during the injection is 20 to 30 %. No appreciable difference was found between co- and counter-injection as far as the reduction of τ_p is concerned, although no many cases were taken with counter-injection [11].

2.2.3 Momentum confinement

The toroidal rotation speed was measured in a series of discharges by a spectrometer with wavelength shift of OVIII lines on a NBI beam path [14]. For a constant value of plasma density and heating power, the peak rotation speed just before the onset of H_α PD has a linear correlation with the ion temperature as shown in Fig. 2.17.

The rotation speed measured by the Doppler system is consistent with the toroidal phase velocity of the B_p fluctuation. The points at high $T_i(0)$ correspond to the H-mode discharge and the lower $T_i(0)$ to the L-mode dishcarge because the points shown in Fig. 17 are for almost the same heating power. Data for limitered discharges are also plotted on the same line. This suggests that the phenomena, at least in the central region of the plasma, are continuous from limitered discharges to H-mode discharges. Discharges with good confinement have a large rotation velocity, suggesting a close relationship between energy confinement and momentum confinement.

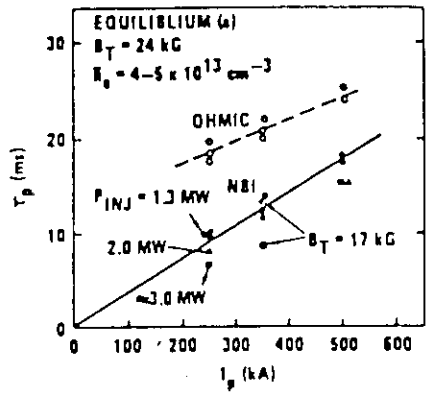

Fig. 2.15 Particle confinement time τ_p versus I_p at $\bar{n}_e$=(4-5)x10^{13} cm^{-3} for neutral-beam injection and Ohmic discharges, in which the plasma is in contact with the primary limiter only (equilibrium (a)).

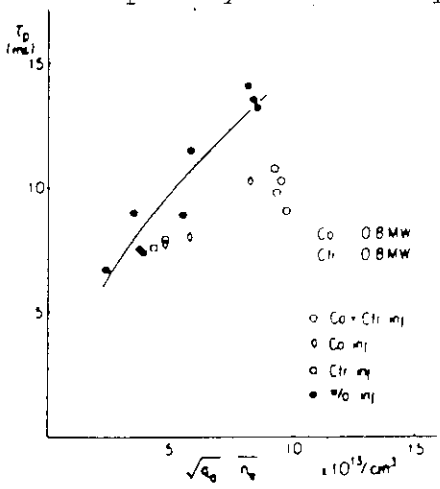

Fig. 2.16 Particle confinement time versus normalized density $\sqrt{q}\bar{n}_e$.

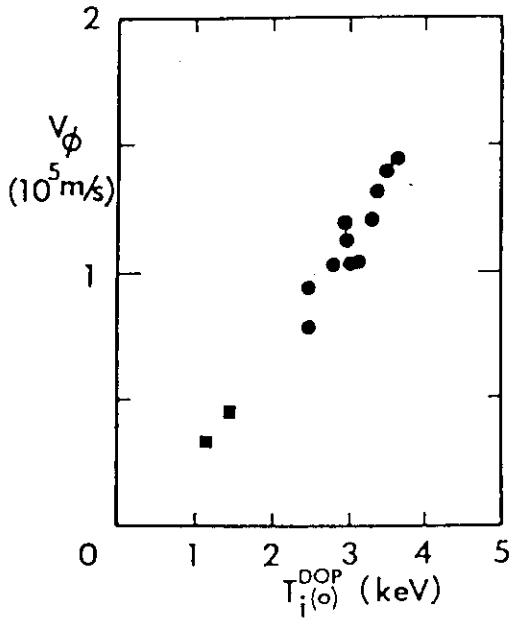

Fig. 2.17 Toroidal rotation speed vs. central ion temperature. (●) Divertor discharge, (■) limiter discharge, P_{inj}=4.5-5.0 MW, n_e=5-7x10^{13} cm^{-3}, I_p=750-830 kA, B_T=2.0-2.6 T.

2.3 R and D programme

No contribution

2.4 Impact on INTOR design and R&D needs

According to the data base described in the preceding sections, the energy confinement properties of INTOR are estimated as shown in $\bar{n}_e$- τ_E diagram of Fig. 2.18.

That is, the grobal energy confinement time of Ohmically heated plasmas with gas fueling follows as neo-Alcator scaling in the low density regime and saturates in the higher density regime. Using the interpretation of the reference [12] for this saturation, the characteristic density $\bar{n}_s$ is proportional to the quantity $\sqrt{a}B_T/Rq\sqrt{T}$. Since the $\bar{n}_s$-value of INTOR is nearly equal to that of D-III for the same $q\sqrt{T}$, the $\bar{n}_e$- τ_E diagram of INTOR is similar to that of D-III as shown in Fig. 2.18. Therefore, the various confinement times of INTOR at the electron density of 1.4×10^{14} cm^{-3} are estimated as follows;

$\tau_{E,OH}$ for gas fuelled Ohmic plasma ---------- 1.2-1.6 sec

$\tau_{E,L}$(L-mode) for gas fuelled limiter plasma --------- 0.7-1.0 sec

$\tau_{E,D}$(H-mode) for gas fuelled divertor plasma
$\tau_{E,D}$(P-mode) for pellet fuelled limiter plasma } ---- 1.4 sec
$\tau_{E,D}$(H-mode) for pellet fuelled divertor plasma

However, the data base in the high density regime of $0.9\text{-}1.4\times10^{13}$ cm^{-3} is not sufficient for exact extrapolation. In D-III, the high power heating data in this regime have not been realized by this time, and also the Murakami coefficient of INTOR is larger than that of D-III. Therefore, the confinement properties in this regime have to be studied in the future. At last, the degradation of the confinement time in the ICRF heating is better or, at least, not larger than that in the NBI heating.

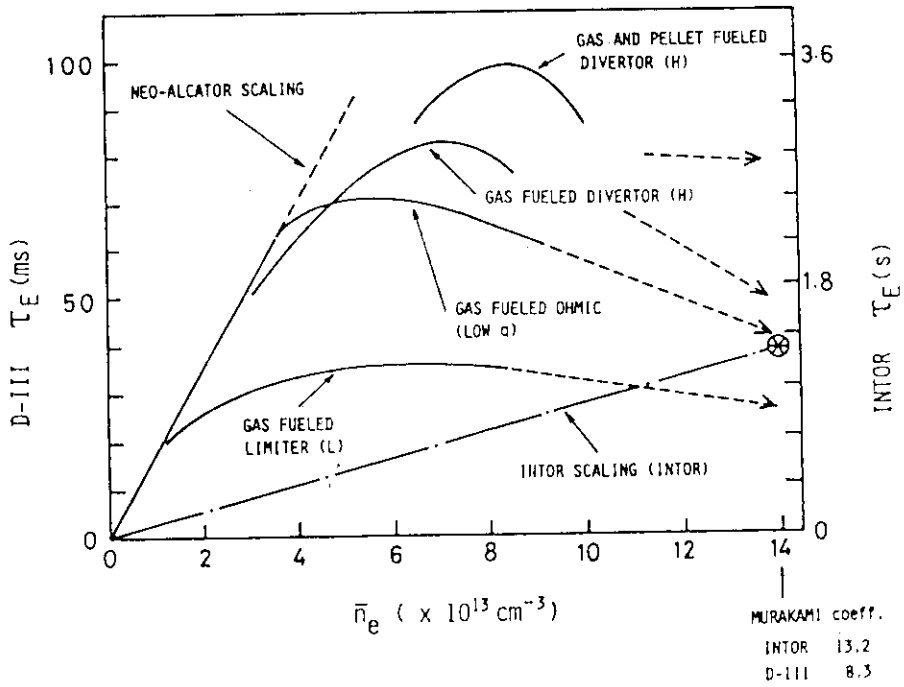

Fig. 2.18 The energy confinement properties of INTOR estimated by the data base.

References for section 2

[1] a) NAGAMI, M., YOKOMIZO, H., SHIMADA, M., YOSHIDA, H., IOKI, K., et.al.; Nuclear Fusion 22 (1982) 3
b) NAGAMI, M., YOSHIDA, H., SHINYA, K., JAHNS, G., YOKOMIZO, H., et.al.; JAERI-M 9589 (1981)

[2] a) MAEDA, H., SENGOKU, S., KIMURA, H., OHTSUKA, H., OHASA, K., et.al.; in Plasma Physics and Controlled Nuclear Fusion Research (Proc. 7th Int. Conf. Innsbruck, 1978) Vol. 1, IAEA, Vienna (1979) 377
b) DIVA GROUP; Nuclear Fusion 20 (1980) 271
c) YAMAMOTO, S., SENGOKU, S., MATSUDA, T., MATSUMOTO, H., OHASA, K., et.al.; Jpn. J. Appl. Phys. 19 (1980) L413
d) YAMAUCHI, T., SHOJI, T., FUNAHASHI, A., KUMAGAI, K.; Nuclear Fusion 20 (1980) 1381

[3] a) KONOSHIMA, S., FUJISAWA, N., MAENO, M., SUZUKI, N., YAMAMOTO, T., et.al.; J. Nucl. Mater. 76&77 (1978) 581
b) TAKEUCHI, H., SHOJI, T., FUNAHASHI, A., TAKAHASHI, K.; J. Phys. Soc. Japan 44 (1978) 1363
c) SHOJI, T., YAMAMOTO, T., FUNAHASHI, A., SHIMADA, M., FUJISAWA, N., et.al.; JAERI-M 9799 (1981)

[4] SHOJI, T., FUNAHASHI, A., HOSHINO, K., KASAI, S., KAWAKAMI, T., et.al.; Proc. of the 11th Europ. Conf. on Controlled Fusion and Plasma Physics (Aachen) 1 (1983) 55

[5] KAWAHATA, K., FUJITA, J., MASE, A., NISHIZAWA, A., NODA, A.; Proc. of the 11th Europ. Conf. on Contrtolled Fusion and Plasma Physics (Aachen) 1 (1983) 239

[6] a) NAGAMI, M., and the JAERI TEAM, OVERSKEI, D., and the GA TEAM; in Plasma Physics and Controlled Nuclear Fusion Research (Proc. 9th Int. Conf. Baltimore, 1982) Vol. 1, IAEA, Vienna (1983) 27
b) NAGAMI, M., KASAI, M., KITSUNEZAKI, A., KOBAYASHI, T., KONOSHIMA, S., et.al.; Nuclear Fusion 24 (1984) 183

[7] a) SHIMOMURA, Y., SUZUKI, S., YAMAMOTO, S., MAENO, M., OHASA, K., et.al.; JAERI-M 9065 (1980)
b) YAMAMOTO, S., MAENO, M., SENGOKU, S., SUZUKI, N., KASAI, S., et.al.; Proc. 9th Conf. on Plasma Physics and Controlled Nuclear Fusion Research (Baltimore) 1 (1982) 73

[8] NAGAMI, M., KASAI, M., AIKAWA, H., KITSUNEZAKI, A., KOBAYASHI, T., et.al.; Ptroc. 11th Europ. Conf. on Controlled Fusion and Plasma Physics (Aachen) 1 (1983) 115

[9] a) KIMURA, H., ODAJIMA, K., SENGOKU, S., OHASA, K., SUGIE, T., et.al.; Nuclear Fusion 19 (1979) 1499
b) MATSUMOTO, M., KIMURA, H., ODAJIMA, K., HOSHINO, K., KASAI, S., et.al.; Nuclear Fusion 24 (1984) 283

[10] HOSHINO, K., YAMAMOTO, T., FUNAHASHI, A., SUZUKI, N., et.al.; JAERI internal report

[11] MATSUMOTO, H., KIMURA, H., SENGOKU, S., SUZUKI, N., OHASA, K., YAMAMOTO, S.; Nuclear Fusion 22 (1982) 840

[12] GOLDSTON, R.; in Plasma Physics and Controlled Nuclear Fusion 26 (1984) 87

[13] SENGOKU, S., ABE, M., HOSHINO, K., ITOH, K., KAMEARI, A., et.al.; 10th Conf. on Plasma Physics and Controlled Nuclear Fusion Research (London, 1984, IAEA), IAEA-CN-44/J-I-1

[14] KITSUNEZAKI, A., ABE, M., HIRAYAMA, T., HOSHINO, K., KAMEARI, A., et.al.; ibid, IAEA-CN-44/AI-4

[15] a) SHIMADA, M., et.al.; Nuclear Fusion 22 (1982) 643
b) SENGOKU, S., et.al.; Nuclear Fusion 24 (1984) 415
[16] MORI, M., HASEGAWA, K., HONDA, A., HOSHINO, K., ISHIBORI, I., et.al.; 10th Conf. on Plasma Physics and Controlled Nuclear Fusion Research (London, 1984, IAEA), IAEA-CN-44/F-i-3
[17] TOI, K., WATARI, T., OHKUBO, K., KAWAHATA, K., NODA, N., et.al.; ibid, IAEA-CN-44/F-III-2

3. Neutral Beam Heating and Current Drive

3.1 Current INTOR plasma design assumptions and parameters

High temperature plasma of $T_e(0) \sim 5$ keV and $T_i(0) \sim 5.5$ keV are producted at $n_e \gtrsim 6.5 \times 10^{13}$ cm^{-3} with $\sim$8MW NBI heating in Doublet III [1]. Heating of the INTOR plasma to ignition conditions seems feasible using neutral beam energies achievable with positive-ion-based technology (150-200 keV per deuteron). In the present INTOR design concept, the bulk heating system is ICRH, with NBI specified as the backup.

3.2 Data base

3.2.1 Neutral beam heating

3.2.1.1 Experimental status

JFT-2 was shut down in June 1982 after 10 years operation. A 2-MW neutral-beam injection (NBI) system and a 1-MW ion cyclotron range of frequency (ICRF) system were installed on JFT-2. The injectors are run in H_2. The NBI system consists of a co- and a counter-injector with an injection angle of 36° with respect to the plasma axis. Each beam line provides an ion beam of 65 A at 40 kV and species mix is 60 % H_1^+, 30 % H_2^+ and 10 % H_3^+. In the last phase of JFT-2 Experiments, the effects of intense heating with neutral-beam injection on transport processes were studied, and the following results obtained [2,3]: (1) Typical global energy confinement time is about 10 ms in beam-heated discharges of 0.3 to 1.7 MW, and about 20 ms in only Ohmically heated discharges under optimum conditions. The global energy confinement time in beam-heated plasma depends weakly on the plasma density and the toroidal magnetic field, but increases with plasma current. Up to a power level of 2.2 MW (1.7 MW NBI and 0.5 MW ICRF), the increase in poloidal beta is roughly proportional to the net input power. (2) The global particle confinement in beam-heated discharge is 20-30 % lower than for Ohmic heating. (3) The density clamp observed during beam heating is due to decreased recycling of neutrals from the plasma boundary. (4) In the case of the two beams, 1MW co-beam and 1 MW counter-beam, the increment of poloidal beta is additive. The toroidal plasma rotation induced by the momentum input associated with NBI is unimportant in transport processes. (5) No rapid impurity accumulation occurs during counter-injection. (6) Sawtooth oscillations change into the continuous mode when β_p exceeds a critical value [4].

At present, tokamak experiments are carried out on JFT-2M [5], which went into operation in April 1983 with NBI and ICRF heating experiments just started, and DIII, a joint Japan-USA experiment.

The NBI system of JFT-2M consists of a co- and a counter-injection with an injection angle of 38° with respect to the plasma axis. Each injector is capable of delivering 1.2 MW to the plasma for 200 ms at a source voltage E_b of 40 kV and species mix is 72 % H_1^+, 22 % H_2^+ and 6 % H_3^+.

The NBI system of DIII is designated to provide substantial auxiliary heating to a high density ($\bar{n} \sim 1 \times 10^{14}$ cm^{-3}) non-circular cross-section plasma. Near-perpendicular injection at approximately 27° to a radius vector at the plasma centerline, together with high energy hydrogen beams, is used to ensure

substantial heating of the plasma core. Each ion source, when operating at a nominal 80 kV extraction voltage, delivers a beam whose approximate species mix is 60 % H_1^+, 30 % H_2^+ and 10 % H_3^+ to a close-coupled neutralizer [6]. In DIII, energy confinement of beam-heated divertor and limiter discharges has been studied, and the following results obtained [7]: Observation of the intensity of the recycling particle flux at the main plasma edge for various limiter and divertor discharges indicates that the gross energy confinement of beam-heated discharges is closely related to the intensity of the edge particle flux. In limiter discharges, the global particle confinement time and the energy confinement time τ_E show many similarities: 1) linear I_p dependence at $I_p < 600$ kA, 2) no B_T dependence, and 3) deterioration against injection power. Improvement of τ_E by increasing I_p, for example, is associated with high temperatures at the plasma edge region accompanied by reduced particle recycling. Divertor discharges with low particle recycling around the main plasma show better energy confinement than limiter discharges at high plasma densities. The improvement of τ_E is primarily originated in the reduction of heat transport at the main plasma edge, which is associated with the reduction of recycling particle flux at the main plasma edge. Under certain operation condition, for example, excessive cold-gas puffing, the discharge shows relatively high scrape-off plasma density and strong particle recycling between the main plasma and the limiter. The energy confinement time of these discharges degrades somewhat or reduces completely to that of the limiter discharges. In low-recycling divertor discharges, the central electron and ion temperature is proportional to the injection power, and the plasma stored energy are proportional to $\bar{n}_e P_{abs}$ (scales INTOR scaling). With 4 MW beam injection, high-temperature and high-density plasma were obtained (stored energy up to 280 kJ, $T_e(0) \approx T_i(0) \approx 2.5$-$3.0$ keV at $\bar{n}_e \approx (6-7)\times10^{13}$ cm^{-3}, $\tau_E \approx 70$ ms).

The first ohmic experiment on JT-60 is scheduled in early 1985. Plasma heating experiments with NBI of 20 MW and RF of 10 MW will be initiated in late 1986. One out-standing feature is the achievement of 100 kV, 70 A, 10 s proton beam with a proton ratio of 90 % [8].

3.2.1.2 Theory

a) Theoretical modelling and calculations of neutral beam trapping, penetration, thermalization

For the understanding of NBI heating experiments, both theoretical [9] and numerical [10] (Monte-Carlo) codes to calculate neutral beam trapping and penetration have been developed. The time dependent power deposition profiles [11] are derived by using simple description of the local beam power fractions derived by Stix. Detailed non-time dependent beam power deposition [12] is derived by an orbit following Monte-Carlo code. A new code which is time-dependent orbit following Monte-Carlo code is in progress [13]. Another kind of orbit following Monte-Carlo code to derive the spectrum of charge exchange neutrals which enter into a diagnostic port has been developed to analyze diagnostic results [14].

b) Decay of Poloidal Rotation in a Tokamak Plasma

A relaxation mechanism for the externally excited radial electric field in a tokamak plasma is investigated in the "banana" regime [15]. It is shown that the damping time scale is of the order $\varepsilon^{3/2}/\nu_{ii}q^2$, where ε is the

inverse aspect ratio, ν_{ii} the ion-ion collision frequency, q the safety factor. The plasma in a tokamak is found to have a large effective dielectric constant by a factor q^2/ε^2. The decay of the radial electric field due to toroidal-field ripples in tokamak systems in the banana regime [16]. The characteristics decay time of the field E_r becomes several tens of milliseconds for typical plasma parameters of a tokamak ($n=5.5\times10^{13}$ cm^{-3}, $T_i=10$ keV, $q=2.5$, $\varepsilon=0.25$ and $\delta=0.002$), where $2\,\delta(r)B_0$ represent the magnitude of the field ripple on the magnetic surface r = constant. This value seems to be short enough to neutralize the radial electric field generated during the beam injection heating of the plasma.

3.2.1.3 Comparisons and conclusion

The role of scrape-off and/or boundary layer on plasma confinement in beam-heated discharges was discussed [17,18]. The density clamp phenomena is explained by the following mechanisms. A relatively large amount of injected power is deposited around the plasma boundary and increases the plasma boundary temperature, compared with the Ohmically heated discharge. The increase in sheath potential decreases the reflection coefficient of the incident ion flux onto the wall (or limiter). In addition, the low temperature neutral gas via the gas puffing is ionized near the plasma boundary, including the scrape-off, because the ionization rate of hydrogen increases with the temperature in the range ($T_e \lesssim 100$ eV). Thus, the density clamp occurs. To overcome the density clamp, the intense gas puffing is necessary as above mentioned. The cooling effect due to low temperature neutrals is much less than for Ohmically heated discharges, and the boundary temperature is still high enough to ionize the low temperature neutrals, because the birth profile of fast ions depends on plasma profile and the large amount of the injected power is deposited around the boundary, including the scrape-off. Thus, broader density profiles are inevitably obtained in high density regions. At the same time, the scrape-off density in beam-heated discharge becomes much larger than for the Ohmically heated discharges. The higher plasma density at the plasma boundary region increases the deposition power near the boundary and thus decreases the deposition power of the plasma center. Thus, the density profile control may be one of the key factors in improving τ_E in beam-heated discharges.

By solving the energy balance equations, the electron thermal diffusivity χ_e^{NBI} is estimated for experimental data from the JFT-2 tokamak with neutral beam injection heating [19]. Heat deposition profiles from fast ions to bulk electrons and ions are calculated in detail by an orbit-Monte Carlo code <u>including a scrape-off plasma</u>. The increase in density and temperature near scrape-off layer is supposed to worsen the deposition profile and the estimated χ_e^{NBI} is two to three times that in the Ohmic case without additional heating.

On the other hand, in DIII, density profiles of beam heated discharges are investigated for low- and high-recycling divertor discharges as well as for limiter discharge [7]. The large variation appears in the edge region. The existance of a substantial edge plasma density for high-density limiter discharges was found. In Doublet III NBI conditions (near-perpendicular high-energy hydrogen beam injection), the beam power deposition at $r < 0.5a$ changes less than about 10 % for the n_e profile variation shown here for the divertor and limiter discharges with the same $\bar{n}_e$. The change in the power deposition profile is, therefore, not responsible for any change in energy

confinement time with different discharge conditions but the same n_e.

3.2.2 Neutral beam current drive

3.2.2.1 Experimental status

There is no investigation of tokamak current drive using neutral beams in Japan. Only in Heliotron E [20], the experiment of neutral beam current was done. Induced toroidal plasma current flows in the same direction as neutral beam. Component of beam induced plasma current is 1.1 kA under neutral beam injection of 1 MW (28° injection, P_{abs}=0.5 MW) and observed toroidal plasma current should be composed of two origins, beam induced "Ohkawa" current and the diffusion-driven neoclassical "bootstrap" current.

3.2.2.2 Theory

A current drive scheme based on combining neutral beam-injection and ICRF heating is investigated [21]. The neutral beam injection mainly supplied toroidal momentum and is sustained by ICRF wave heating. The current is generated with sufficient efficiency and can sustain the tokamak plasma in a steady state. In addition, the current-drive scheme without beam-ions injected by NBI, instead, with alpha-particles produced due to the fusion reaction is investigated [22].

3.3 R and D programmes

3.3.1 On-going programmes and expected advancements

a) Cyclotron instability due to neutral-beam-injection

In the JFT-2M tokamak, a neutral-beam-injection (NBI) method to modify the distribution function $f(\vec{v})$ in a velocity space of injected beam particles in a tokamak plasma has been developed. The method, multiple-short-pulse method, is characterized by the repetition period t_r and the pulse length t_l, and is expected to be a useful tool for the detailed investigation of slowing down process of injected beam particles [23] and of NBI effects on plasma confinement. We have excited waves with this method in the ion-cyclotron range of frequencies (ICRF) [24] due to beam-plasma interactions by an controllable manner [25] (Fig. 1). The theoretical analysis [26] has shown that the high energy beam particles can excite the Alfven wave eigenmodes in the ICRF if the beam density exceeds a threshold and that the excited wave may contribute to the nonclassical energy transfer from the beam particles to the bulk plasma particles. It is very important to clarify the role of the excited wave on power balance in tokamak plasmas and the effects on plasma confinement.

b) Simultaneous heating of NBI and ICRF

In the JFT-2 tokamak, significant plasma heating is observed with simultaneous NBI and ICRF heating. With a net power of 2.2 MW (1.7 MW NBI and 0.5 MW ICRF) into D^+ plasma at a plasma density of 6×10^{13} cm^{-3}, the central ion temperature increases from 0.4 to 1.4 keV [2]. In the JFT-2M tokamak, simultaneous heating of NBI and ICRF has been also performed [27]. A theoretical analysis of ICRF wave heating in a plasma with neutral-beam injection (NBI) is performed [28]. Wave propagation and absorption are

examined kinetically in the presence of a high-energy ion beam component. The following findings are reported: 1) the wave coupling efficiency does not deteriorate by the beam; 2) co-operative heating is to be expected, and 3) selective heating of high-energy ions is possible.

c) Role of particle-wave interaction in the beam-heated H-mode discharges [29]

The energy confinement time of ICRF heated plasma in limiter discharges is better than that of NBI heated plasma, if we take account of energy loss due to impurity radiation. Experimental results obtained in JFT-2M show that time behaviors of toroidally averaged main chamber $H\alpha/D\alpha$ line radiation and line averaged plasma density during ICRF heating are similar to those of beam-heated H-mode discharge obtained in ASDEX and DIII. Theoretical analysis [26,30] have shown that the wave in the ICRF can be excited owing to anisotropic non-maxwellian energetic ions in tokamak configurations. In fact, we have excited the waves in the ICRF due to beam-plasma interaction [25]. There is some evidence for particle wave interaction during the beam heated H-mode discharge [31]. These studies suggest that it is important to clarify the role of excited wave in the ICRF on plasma particle confinement and the energy confinement in beam heated H-mode discharge.

d) Development of negative ion source

Out of many methods to produce negative ion beams, volume production method [32] is the most attractive one, because this method needs no cesium handling and the structure of the ion source is simple enough to scale up. As a first step of the development of negative ion source, at JAERI, the yield of volume produced H^- ions is investigated in several configurations of multiple line cusp plasma source as function of plasma density, gas pressure, electron temperature and other operating parameters [33]. At optimum conditions, H^- ion beam with a current density of 12 mA/cm^2 is extracted at beam energy of 10 keV for 0.2 s.

3.3.2 Additional R and D needs

The impurity problem is very severe during ICRF heating, especially, with second harmonic resonance heating method [27]. The investigation of impurity control during ICRF heating has just begun [34].

On the other hand, the reactor grade plasma has been succesfully obtained in DIII with high power neutral beam injection [1]. Continued support of the negative ion development program [33] is needed even if the bulk heating system for INTOR is ICRF.

For improvement of heating efficiency of NBI, the development of various kinds of NBI techniques (for example, multiple-short-pulse injection [25], changing beam energy within a pulse [33] and so on) is necessary.

In the JFT-2M tokamak, we have excited the Alfven wave eigenmode in the ICRF due to beam-plasma interaction in a controllable manner [25]. Magnetic compression heating may invert the velocity distribution of alpha particles and lead to the possibility of exciting velocity space instability [35]. More detailed experimental investigation is necessary to clarify the role of beam-driven instability on plasma confinement and energy balance in tokamak plasma.

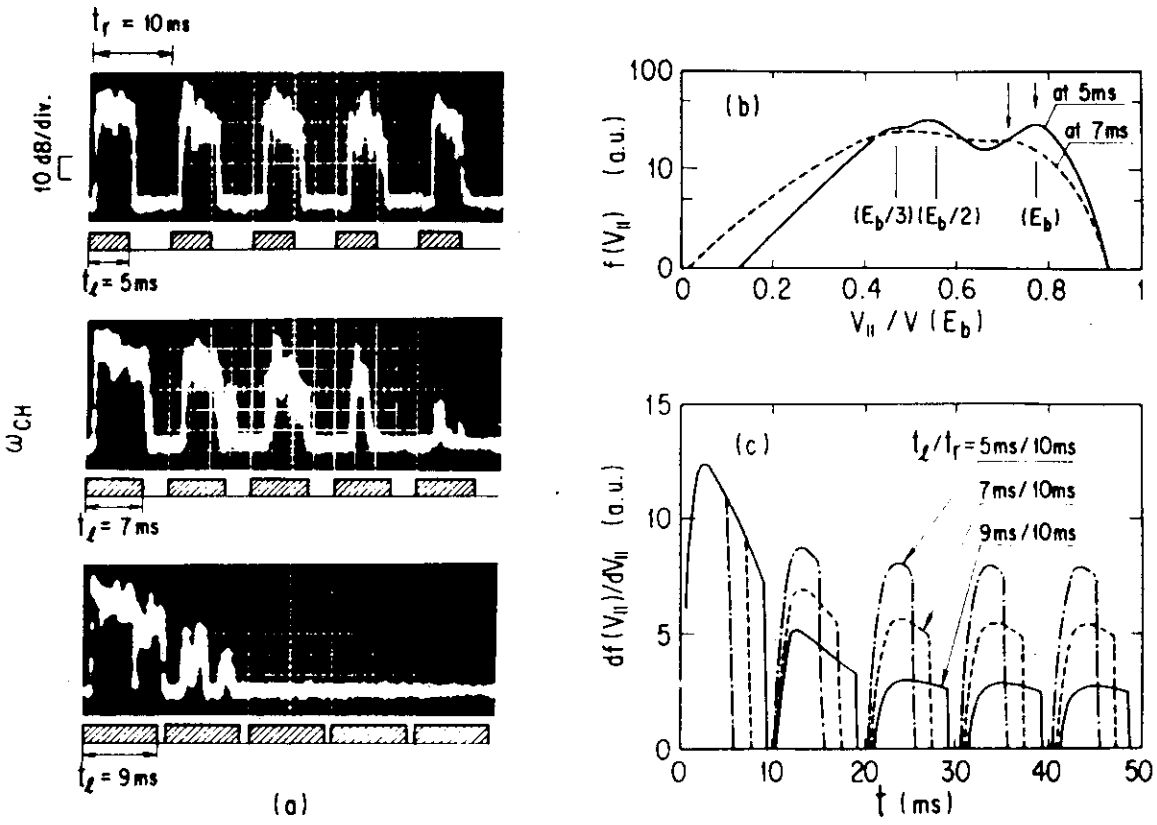

Fig. 1 (a) Relation between rf-oscillation amplitude ($\omega/2$ =19MHz) and beam pulse length (t_1=5ms, 7ms and 9ms) when the pulse repetition period is fixed (t_r=10ms). B_T=1.25T, I_p=150kA, $\bar{n}_e$=1.5x10^{13} cm^{-3}, n_H/n_D=0.3-0.5, E_b=35keV, and I_b=50A (0.75MW co-injection). (b) Calculated parallel velocity distribution function $f(v_{\parallel})$ at the plasma center. In this case, beam is shut off at t=5 ms. Calculation parameters are as follows: T_e=800eV, T_i=600eV, $n_e(0)$=2.25x10^{13} cm^{-3}, E_b=35kV, I_b=50A and beam power fraction P(E):P(E/2):P(E/3)=6:3:1. (c) Time behavior of slope of parallel velocity distribution function defined between two points denoted by arrows in (b) for MSP cases (t_1=5ms, 7ms and 9ms) and t_r=10ms.

References for section 3

[1] KITSUNEZAKI, A., et al., "High Pressure Plasma with High Power NBI Heating in Doublet III", in Plasma Physics and Controlled Nuclear Fusion Research (Proc. 10th Int. Conf. London, 1984) AI-4.
[2] YAMAMOTO, S., et al., "Transport Studies in the JFT-2 Tokamak", in Plasma Physics and Controlled Nuclear Fusion Research (Proc. 9th Int. Conf. Baltimore, 1982) Vol. 1, IAEA, Vienna (1983) 73.
[3] SHIMOMURA, Y., et al., "Neutral Beam Heating at JAERI", in Heating in Toroidal Plasma (Proc. 3rd Joint Varenna-Grenoble Int. Symp. Grenoble, 1982) Vol. 1 (1982) 27.
[4] YAMAMOTO, S., et al., "Magnetohydrodynamic Activity in the JFT-2 Tokamak with High-Power Neutral-Beam-Injection Heating", Nucl. Fusion 21 (1983) 993.
[5] SHOJI, T., et al., "Results from the JFT-2M Experiments", in Controlled Fusion and Plasma Physics (Proc. 11th Europ. Conf. Aachen, 1983) paper A08.
[6] COLLERAINE, A., et al., "Preliminary Neutral Injection Experiments on DIII", in Heating in Toroidal Plasma (Proc. 3rd. Joint Varenna-Grenoble Int. Symp. Grenoble, 1982) Vol. 1, (1982) 49.
[7] NAGAMI, M., et al., "Energy Confinement of Beam-Heated Divertor and Limiter Discharges in Doublet III", Nucl. Fusion 24 (1984) 183.
[8] MATSUDA, S., NAGASHIMA, T. and SHIMOMURA, Y., "Plasma Heating System for JT-60", in 4th Int. Symp. on Heating in Toroidal Plasma (Rome, 1984).
[9] OHTSUKA, M., et al., "A Neutral Beam Deposition Code for Non-Circular Tokamak Plasma", J. Comp. Phys. 52 (1983) 219.
[10] TANI, K., et al., paper in preparation.
[11] HIRAYAMA, T., et al., "Numerical Transport Studies of Injected Titanium into Doublet III Beam Heated Discharges", GA-A17406, (1984).
[12] TANI, K., AZUMI, M., OHTSUKA, M., Proc. Joint Varenna-Grenoble Int. Symp. Heating in Toroidal Plasma Grenoble 1 (1978) 31.
[13] TANI, K., AZUMI, M., et al., paper in preparation.
[14] AZUMI, M., et al., paper in preparation.
[15] TUDA, T., "Decay of Poloidal Rotation in a Tokamak Plasma", J. Phys. Soc. Japan 39 (1975) 1358.
[16] TUDA, T., "Ripple Diffusion and Decay of Poloidal Rotation in a Tokamak Plasma", Nucl. Fusion 15 (1975) 541.
[17] YAMAMOTO, S., "JFT-2 Experiments with Additional Heating", in Proc. of US-JAPAN Workshop on "Anomalous Transport and Critical Beta Value", March 1983.
[18] Annual Report of the Fusion Research Center for the Period April 1, 1982 to March 31, 1983, JAERI-M 83-182 p.18.
[19] OKAMOTO, M., et al., "Electron Thermal Diffusivity in JFT-2 Tokamak with NBI Heating", Jpn. J. Appl. Phys. 22 (1983) 686.
[20] BESSHOU, S., et al., "Observation of Beam-Induced Toroidal Plasma Current and Neoclassical Current under Neutral Beam Injection Heating in Heliotron E", Plasma Physics and Controlled Fusion 26 (1984) 565.
[21] OKANO, K., INOUE, N., UCHIDA, T., "Scaling Law of ICRF-Wave-Enhanced Beam-Driven-Current", Nucl. Fusion, 23 (1983) 235.
[22] OKANO, K., INOUE, N., UCHIDA, T., SUGIHARA, R., OGAWA, Y., "Current Generation by Interaction of Alpha Particles with ICRF Waves", in Plasma Physics and Controlled Nuclear Fusion Research (Proc. 9th Int. Conf. Baltimore, 1982) Vol. 2, IAEA, Vienna (1983) 557.

[23] W VII-A Team and NI Group, "Ion Heating in the Stellarator W VII-A", in Controlled Fusion and Plasma Physics (Proc. 11th Europ. Conf. Aachen, 1983) paper E33.
[24] OHTSUKA, H., et al., "Observation of ICRF Waves During Neutral Beam Injection in Tokamaks", JAERI-M 84-150.
[25] YAMAMOTO, S., et al., "Plasma Heating by Multiple-Short-Pulse Neutral Beams", in Plasma Physics and Controlled Nuclear Fusion Research (Proc. 10th Int. Conf. London, 1984) F-IV-10.
[26] ITOH, S.-I., ITOH, K. and FUKUYAMA, A., "Beam-Driven ICRF Instability and Associated Nonclassical Transport in Tokamak" Research Report HIFT-89 (Hiroshima Univ., 1984). Plasma Physics and Controlled Fusion 26 (1984) in press.
[27] ODAJIMA, K., et al., "Second Harmonic ICRF Heating Experiment in the JFT-2M Tokamak", in 4th Int. Symp. on Heating in Toroidal Plasma (Rome, 1984).
[28] ITOH, S.-I., FUKUYAMA, A. and ITOH, K., "Simultaneous Heating by ICRF Wave and Neutral-Beam Injection", Nucl. Fusion 24 (1984) 224.
[29] YAMAMOTO, S., ITOH, K., TAKIZUKA, T. and OHTSUKA, H., paper in preparation.
[30] MIKHAILOVSKII, A.B., Theory of Plasma Instabilities (Consultants Bureau, New York) Vol. 2.
[31] STEINMENTS, K., et al., "Non-thermonuclear Neutron Production in Hydrogen-Beam-Heated ASDEX Plasma", in Controlled Fusion and Plasma Physics (Proc. 11th Europ. Conf. Aachen, 1983) A07.
[32] BACAL, M., et al., Rev. Sci. Instrum., 50 (1979) 719.
[33] OKUMURA, Y., et al., "Development of High Performance Neutral Beam Injection at JAERI", in Plasma Physics and Controlled Nuclear Fusion Research (Proc. 10th Int. Conf. London, 1984) H-I-5.
[34] MORI, M., et al., "High Power ICRF Heating Experiments in the JFT-2M Tokamak", in Plasma Physics and Controlled Nuclear Fusion Research (Proc. 10th Int. Conf. London, 1984) F-I-3.
[35] YAMAZAKI, K., OKAMOTO, M., "Sufficient Stability Condition for Alpha-Driven Velocity-Space Modes in Compression-Heated Tokamaks", Nucl. Fusion 23 (1983) 375.

4. Operation Scenarios

4.1 Physics design assumptions and parameters (Phase Two A)

The INTOR operation scenario is drawn in the following figure. The maximum loop voltage available for plasma formation and current initiation is 35 V and the provision has been made for 10 MW of electron cyclotron heating to assist current rise and to minimize the volt-seconds needed in the initial phase. A duration of the Ohmic heating phase of 10 s appears to be reasonable. Heating to ignition in 15-20 s by 50 MW of ion cyclotron wave power is now the reference option. The length of the burn phase is maintained 200 s, which is about a fifth of the global skin time in INTOR . Both of the cooling-down time and the current ramp-down time are also 15-20 s, while the dwell time is chosen to be 20 s.

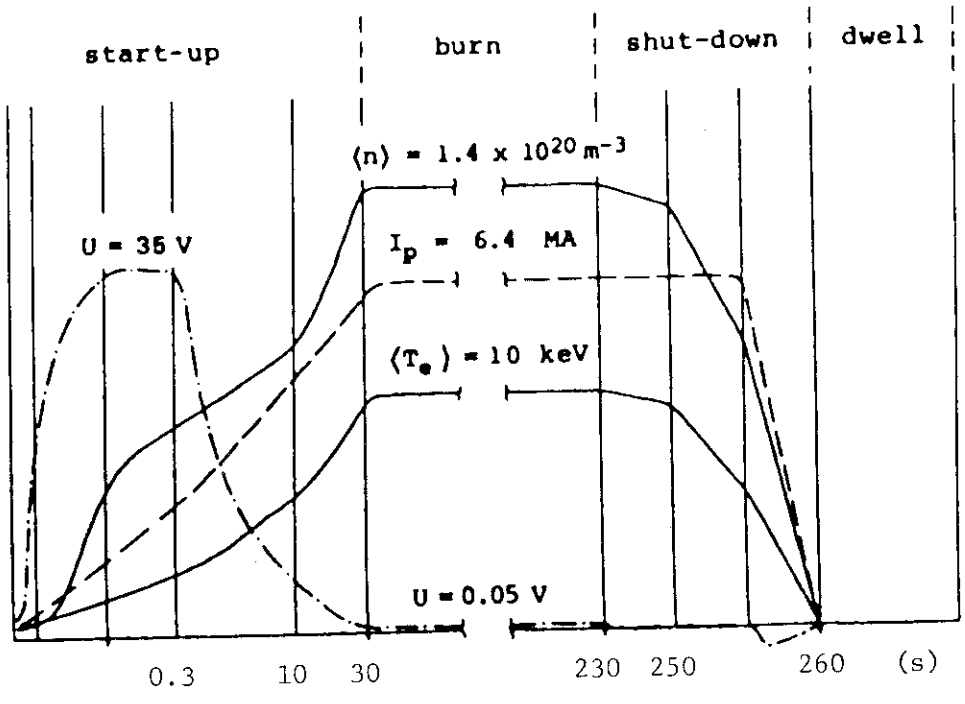

INTOR operation scenario

4.2 Data base

Detailed operation scenario of INTOR seems difficult now to be credibly specified. From experimental experiences on JFT-2 and JFT-2M, some comments are presented. They comes from medium size tokamaks, but furthermore informations will be taken from the large tokamaks such as JT-60.

Vacuum condition

On JFT-2 [1] and JFT-2M [2], the chamber wall and limiter are cleaned with TDC and gettering with titanium. To obtain a stable and clean plasma, the vacuum condition is a key factor. Judgement on whether experiments can start or not is partly based on the mass analysis data during TDC, that is, the production rate of M/e = 18 should be less than 10^{-4} Torr l/sec. On INTOR, the measure of vacuum conditions must be also necessary and it must be solved that what method is applicable for vacuum conditioning, what measurement is appropriate and how to decide the critical value.

Plasma production and control

Some comments on fundamental items to be solved are given.

a) Plasma current control

In the breakdown phase of JFT-2, pre-ionization with ECRH decreased the breakdown voltage to about half value of that without ECRH [3]. The calculated inductive part of loop voltage agreed well to the measured one. So with a sufficient pre-ionization such as ECRH, plasma current may be built up easily with comparatively low loop voltage corresponding to the inductive part. After the breakdown, plasma current is planned to be raised with a rate of 1 MA/sec. This rate is not so high in comparison with results in JFT-2M and D-III. But the problem of current rise rate will be solved in JT-60 with a movable limiter. Before plasma current reaches near q=3, severe mhd instabilities may not appear. Because kink instabilities of higher than m/n = 3/1 mode have only a small growth rate. Therefore in the first phase, plasma current can be raised up to values between q=4 and q=3. But near q=3, kink instability of m/n=3/1 and dangerous tearing mode of m/n = 2/1 will be excited. Here, careful control of plasma parameters to overcome this barrier may be required, such as plasma density, plasma position and so on. In JFT-2M, initial current is raised with the rate of 1 MA/sec up to q=3.5, then plasma density is ramped up enough under nearly constant plasma current. Then rising rate of about 0.5 MA/sec is now necessary to run through the q=3 barrier. Key factors to overcome the barrier seems to be comparatively high density, clean plasma and moderate current rising rate. The barrier of q=2 is too hard to overcome [4,5]. But there is a wide accessible region between q=2 and q=3, so plasma current setting higher than 6.4 MA will be possible in INTOR.

To obtain a stable high beta plasma, current profile control may be one of necessary techniques. Up to now, sufficient experimental data are not yet obtained. This is one of important R and D items.

b) Position control

Position of outermost magnetic surface is estimated from various

electro-magnetic measurements and checked by the simulation code on plasma equilibrium. If a reliable monitor of the position is established, feedback control system should work according to reference command. In this region, many experiences have been stored and necessary technologies have been developed.

Here, one residual problem is control of the vertical instability. On D-III, capability of non-circular plasma to obtain a high beta plasma has been demonstrated and elongation of 1.8 was achieved [6]. On JFT-2M, elongation of 1.5 was also accomplished. But capability of vertical position control depends on the passive stabilization effects of vacuum chamber, poloidal coils and so on. Therefore it depends on the passive stabilization effects of inner compositions in INTOR that whether a stable divertor plasma with elongation of 1.6 can be obtained or not.

c) Shaping control

Control of plasma shape is conductd with adjustment of poloidal coil currents, which is reduced from the equilibrium simulation. Here, it seems not to be necessary that the same elongated plasma shape is maintained throughout a duration time. Especially in the initial build-up phase, nearly circular plasma setting may be a safety choice. Then, a desired plasma shape can be established easily. On JFT-2M and D-III, this method is used to control the plasma shape from a circular plasma to a D-shape plasma or to a divertor plasma.

d) Density Control

Controllable region of plasma density is determined by the density limit coming from the major disruption. The density limit depends strongly on cleanliness of plasma, because large radiation loss power triggers the major disruption. So a good monitor in density control is radiation loss power by a bolometer. One method to control plasma density is the gas puffing with the piezo-electric valve and another one is the pellet injection. If there is prepared a reliable density monitor, feedback control of the density may be better than the pre-programming control. Because gas injection rate to get a desired density depends on the recycling rate and the particle confinement time. But in some conditions, intense gas puffing enhances the mhd instability or degrades confinement property, so careful control may be required. The pellet injection has demonstrated the advantage of central fuelling to obtain a higher density and good confinement [7,8], but more development in pellet speed should be required.

e) Heating control

As a main heating method, ICRF heating and NBI heating have been developed and a high beta plasma was demonstrated with NBI heating [9]. In heating control, not only input power control but control of a high beta plasma are required. Input power control in NBI heating is roughly independent on plasma parameter, so it may be easy with a multi-injection system. But in ICRF heating, the loading resistance depends on electron density, complicate control will be necessary. Though ICRF heating has merits such as high heating efficiency and well developed technology, but there was the problem of impurity contamination. Now adjustment of k spectrum by changing phases among antennae is found to be useful method to suppress

impurity release [10]. Further experiments of high power ICRF heating to obtain a high beta plasma may be required.

Control of a high beta plasma with good reproducibility is not yet established and experiments to get higher beta plasma is under way. Control techniques on current profile or pressure profile must be developed. Furthermore some way to the second stable region predicted from the theory must be found out.

f) Shut-down

Shut-down of plasma is an inverse process of start-up. So soft landing of plasma is not so difficult. First, heating power is diminished together with density decrease. Secondly, plasma current is quenched with density decrease. Through this shut-down process, the density must be kept within the density limit, and plasma position must be controlled in the same manner at the start-up. Recovery of magnetic energy and fuel and so on are out of scope.

4.3 R & D programme

In JFT-2M, many experiments are planned such as high power ICRF heating, current drive by LH heating supported with ECRH, pellet injection, poloidal divertor and so on. In JT-60, more relevant information on operation scenario will be obtained in near future.

4.4 Impacts on INTOR design

No contribution

References for section 4

[1] SUZUKI, N., IMAI, T., FUJISAWA, N., et al., in Plasma Physics and Controlled Nuclear Fusion Research (Proc. 8th. Int. Conf. Brussels, 1980) Vol. 2, IAEA, Vienna, (1981) 525
[2] SHOJI, T., FUNAHASHI, A., HOSHINO, K., et al., in Controlled Fusion and Plasma Physics (Proc. 11th Europ. Conf. Aachen, 1983) Vol. 1 (1983) 55
[3] JFT-2 GROUP, in Controlled Fusion and Plasma Physics (Proc. 10th Europ. Conf. Moscow, 1981) Vol. 2 (1981) 87
[4] MAENO, M., SUZUKI, N., KONOSHIMA, S., et al., J. Phys. Soc. Jpn. 48 (1980) 273
[5] NAGAMI, M., YOSHIDA, H., SHINYA, K., et al., Nucl. Fusion 22 (1982) 409
[6] YOKOMIZO, H., NAGAMI, M., SHIMADA, M., et al., Nucl. Fusion 22 (1982) 797
[7] GREENWALD, M., GWINN, D., MILORA, S., et al., Phys. Rev. Lett. 53 (1984) 352
[8] SENGOKU, S., ABE, M., HOSHINO, K., et al., in Plasma Physics and Controlled Nuclear Fusion Research (Proc. 10th Int. Conf. London, 1984) Post-dealline paper
[9] NAGAMI, M., and the JAERI TEAM, OVERSKEI, D., and the GA TEAM, in Plasma Physics and Controlled Nuclear Fusion Research (Proc. 9th Int. Conf. Baltimore, 1982) IAEA, Vienna, Vol. 1 (1983) 27
[10] MORI, M., HASEGAWA, K., HONDA, A., et al., in Plasma Physics and Controlled Nuclear Fusion Research (Proc. 10th Int. Conf. London, 1984) IAEA CN-44/F-I-3

5. Burning plasma

5.1 Physics design assumptions and parameters (Phase Two A)

INTOR plasmas in a burn phase are self-ignited with 10 keV of average temperatures, 200 s of a burn period. Ignited plasmas in such a temperature range need some burn controls. INTOR workshop has continuously assessed several burn control schemes from Phase Zero. Some schemes seem promising, however, the final decision has not been made at present. Toroidal ripple effects on alpha particle confinement have also been evaluated in the workshop Evaluations of the alpha particle loss induced by the ripple have not been converged yet. The present limit of the ripple value is 1.2 %.

5.2 Data base

5.2.1 Alpha confinement and thermalization

Ripple loss

The energy loss fraction of alpha particles is less than 1 % of the total fusion power of charged particles in an axisymmetric tokamak reactor with the plasma current above 6 MA, if the plasma pressure profile is not so flat and the relaxation process of suprathermal alphas is classical.

The loss of alphas is mainly due to the ripple of toroidal magnetic field. This ripple loss was studied in detail by means of an orbit-following Monte-Carlo code [1]. Collisionless ripple loss processes of suprathermal alpha particles are numerically investigated and the results agree fairly well with the theoretical prediction [2]; a trapped alpha particle, whose pitch angle ζ is less than ζ_c and banana tip is located in the region of the ripple δ larger than $\delta_c=[(\pi NqA)^{3/2}\rho q']^{-1}$, is lost due to the collisionless stochastic orbit, where N is the number of toroidal coils, q the safety factor, A the aspect ratio, ρ the gyroradius, and the maximum ripple δ_0 is at the outer side of the torus. Although the initial energy of charged fusion products is very high, collisional effects, slowing-down as well as pitch-angle scattering, are very important for the estimation of their ripple-enhanced particle and power losses. The ripple-enhanced banana drift dominates the loss process of alphas. The diffusion coefficient for stochastic loss particles with pitch angle $\zeta < \zeta_c$ is roughly estimated as

$$D^R \sim N(qA)^3(\rho\delta)^2(v/qR) \quad ,$$

and the diffusion coefficient for confined banana alphas with pitch angle $\zeta > \zeta_c$ is approximately given by

$$D^{CB} \sim N^3(qA)^5(\rho\delta)^2\nu \quad ,$$

where R is the major radius and ν is the 90° scattering frequency of alpha with plasma ions. For the INTOR-like plasma parameters with $\delta_0 \sim 1$ %, D^{CB} of 3.5 MeV alphas is of the order of 0.1 m^2/s, which is much larger than D^{NC} (axisymmetric neoclassical diffusion) and much less than D^R. The ripple-enhanced power loss for $\delta_0=1$ % is about 10 % of the total fusion power of charged particles. The effect of ripple on particle loss is very important not only for energetic but also for slowed-down alphas. The fraction of particle loss is about 1.5 to 1.8 times as large as that of power loss for $0.4\% < \delta_0 < 1.5\%$. The wall heat load due to loss alpha particles is localized, and its peak value reaches the order of 1 MW/m^2 if δ_0 exceeds 1 %. This

investigation showed that there is a possibility of realizing the design of tokamak reactors with a realistic field ripple of $\delta_0 \sim 1$ %, permitting 10 % power loss of alpha particles.

Anomalous transport

Above results are obtained by assuming that the relaxation processes of alphas are classical. Alpha-driven Alfven modes may cause an anomalous energy transport from alphas to bulk ions. The velocity inversion of alpha distribution, however, does not appear in an INTOR-like reactor.

Perturbations of magnetic fields and electric fields due to ballooning mode instabilities can enhance the radial loss of alpha particles. ICRF waves in the additional heating phase can affect the alpha confinement and thermalization. It is required to clarify these anomalous transports.

Alpha current drive by ICRF waves

A current-drive method based on the interaction of fusion products (alpha particles) with ICRF waves was proposed [3]. A theoretical scaling law is obtained and confirmed by numerical simulations. A two-dimensional Fokker-Planck code is used to evaluate current-drive efficiency and induced current for the scheme. Calculations are carried out taking into account the spatial profiles of the density and temperature as well as the presence of the particle orbit loss region in a tokamak. It is found that the current induced by the scheme may sustain tokamaks in steady state. The code can also be applied to check a current-drive scheme using the ^{3}He minority ion.

References for subsection 5.2.1

[1] K. Tani, T. Takizuka, M. Azumi, H. Kishimoto, Nucl. Fusion 23 (1983) 657.
[2] R.J. Goldston, R.B. White, A.H. Boozer, Phys. Rekv. Lett. 47 (1981) 647.
[3] K. Okano, N. Inoue, T. Uchida, R. Sugihara, Y. Ogawa, Proc. 9th Int. Conf. on Plasma Physics and Controlled Nuclear Fusion Research, Baltimore 1982, Vol. 2 (IAEA, Vienna, 1983) 557.

5.2.2 Burn control schemes

(I) Introduction

If a confined plasma is reached to ignition where the alpha-particle heating rate balances the power losses, the resulting self-ignited burning plasma is theoretically expected to be thermally unstable. A small temperature rise increases the fusion reaction rate, and unless the energy loss mechanism works sufficiently to balance the energy gain, the temperature will continue to rise until the fusion reaction rate saturates. At the finally reaching stable equilibrium, the output power and the plasma pressure can be such higher than those at ignition. They may require intolerably high power wall loading or uneconomically large magnetic fields to keep high plasma pressure. Hence, the suppression of this thermal instability seems to be essential to realize fusion reactors.

Stabilization methods can be either passive method which is basically self-control mechanism adjusting the power loss (the power gain) in a time-dependent way, or active method which is principally feedback control mechanism monitoring of deviations from equilibrium. One of the passive methods that is control of the temperature by increases in the heat conductivity from operation near the beta limit is specially attractive. However, Speculations about nonlinear oscillation of beta limit applied for thermal runaway can be settled only by an ignited DT experiment. In the meantime, practical proposals for burn control should be developed.

(II) Compression-decompression

One of the practical proposals is active feedback control method performed by the plasma compression-decompression varing the vertical magnetic field. Bromberg et al. [1] point out that plasma free motion in the radial direction stabilizes thermal runaway, and Borrass [2] first suggested the feedback control with plasma compression-decompression. Recently, Ohnishi et al. [3], carried out a one-dimensional plasma model to analyze the active feedback control by the plasma compression-decompression.

The one-dimensional temperatue balance equation including the effects of the plasma compression-decompression is given as

$$3n\left(\frac{\partial}{\partial t} + r\frac{\dot{R}}{R}\frac{\partial}{\partial r}\right)T = -4nT\frac{\dot{R}}{R} + k_e\left(\frac{\partial^2 T}{\partial r^2} + \frac{1}{r}\frac{\partial T}{\partial r}\right) + Q_\alpha - Q_{br} \qquad (1)$$

where k_e is the thermal diffusivity defined by $k_e = n\chi_e$, Q_α and Q_{br} are the alpha heating power and the radiation loss power by bremsstrahlung, respectively, $\dot{R}$ menas the lagrange derevative of R. The vertical magnetic field B_v is given by the Shafranov equation as $B_v = (\mu_0 I_p/4\pi R)(\ln 8R/a - 3/2 + l_i + \bar{\beta}_p)$. In this control scheme, the vertical magnetic field is divided into two terms such as

$$B_v = (B_{\perp o} + \tilde{B}_v)\left(\frac{R_p}{R}\right)^m \qquad (2)$$

where $B_{\perp o}$ is the stationary field, B_v is the varying field, and m is the field decay index. $\tilde{B}_v$ of the controller is then given by

$$\dot{\tilde{B}}_v + \frac{\dot{\tilde{B}}_v}{\tau_D} = -\frac{G}{\tau_D} B_{\perp o} P(t) \tag{3}$$

where G is the control gain and τ_D is the characteristic time. P(t) denotes the deviation of the plasma temperature or a fusion output power from a specified reference value denfined as

$$P(t) = \begin{cases} \dfrac{T_{eff}(t)}{T_{eff\,o}} - 1 & T_{eff} \text{ control} \\ \dfrac{Q_F(t)}{Q_{FO}} - 1 & Q_F \text{ control} \end{cases} \tag{4}$$

Fig. 1a and 1b show the dynamic behavior in the case of T_{eff} control. The temperature is changed stepwise by ±10% of the equilibrium value within 20 cm from the center axis. The T_{eff} controller with G=2 and τ_D=2 sec is applied at the same time that the disturbances are introduced. Fig. 2a and 2b are the dynamics corresponding to Q_F control with the same plasma parameters as in Fig. 1. Fig. 3 and Fig. 4 show the transient behaviors of T_{eff}, Q_F, R and B_v for the T_{eff} control and Q_F control respectively. The signs "+" and "-" stand for the cases of positive and negative disturbances, respectively. The plasma reveals oscillatory decay responses in T_{eff} control, while it recovers its equilibrium by damping the perturbations exponentially in Q_F control. In either case, the relative deviations of the major radius remain within only 1.2 %. The rates of changes of the vertical field are as small as 50 and 100 G/S at the maximum for T_{eff} control and Q_F control, respectively. Thus, feedback control by compression-decompression can suppress thermal runaway initiated by the local disturbances of temperature.

(III) Conclusions and recommendations

It is shown that the thermal runaway can be suppress by the compression-decompression feedback control. The relative deviation of the major radius is within 1.2 %, that means the major radius moves 6.24 cm for INTOR case. Outward and inward shifts of the plasma major radius will compel the scrape-off layer increase for protecting the plasma in contact with a limiter on the midplane. Futhermore, this type of active control will require very accurate informations about the plasma state such as density, temperature and position. Although there are another possibilities for controlling thermal runaway, much works have to be done before the preferred method will be recommended. The passive control due to the beta limit oscillation is particullary atractive because the power production is a weak dependence on the ignition condition. Further progress in this area is expected.

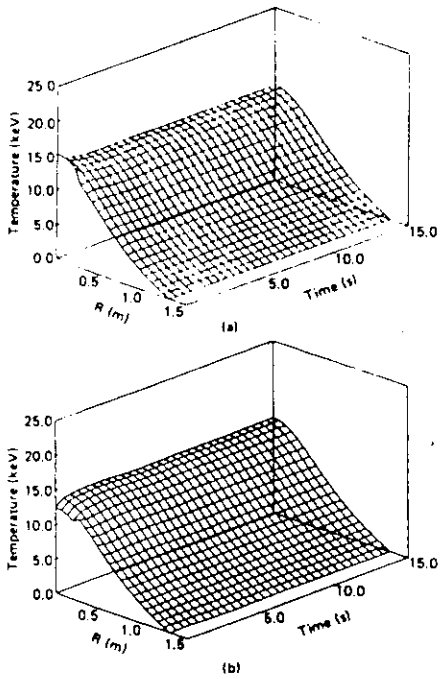

Fig. 1

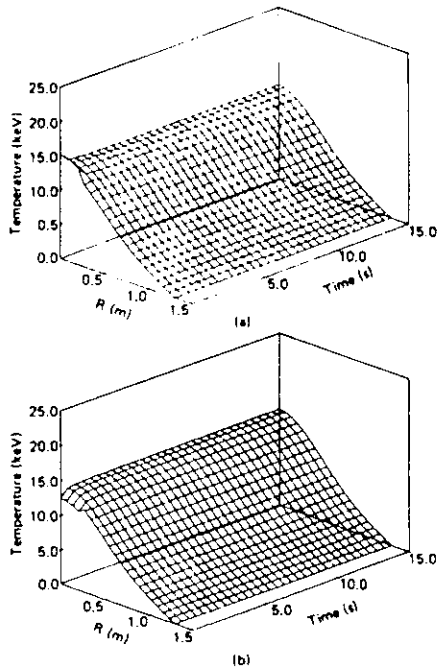

Fig. 2

Fig. 1 Dynamic behaviors when the T_{eff} control (G=2 and D=2 s) is applied at the same time that the disturbances are introduced.

Fig. 2 Dynamic behaviors when Q_F control (G=2 and D=2 s) is applied at the same time that the disturbances are introduced.

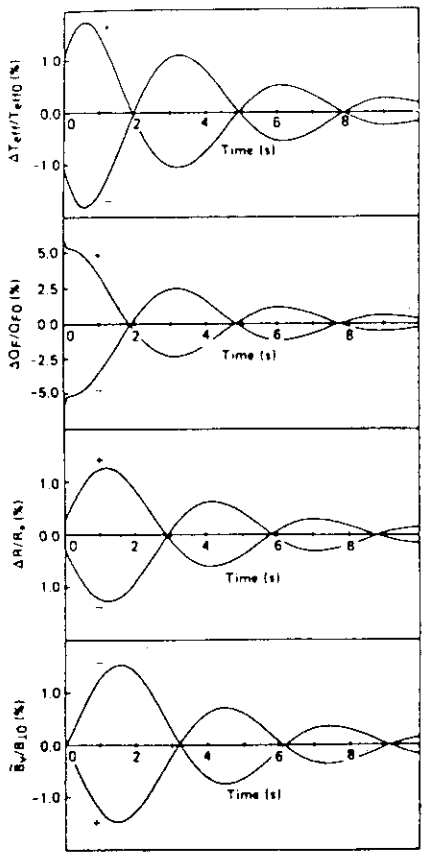

Fig. 3

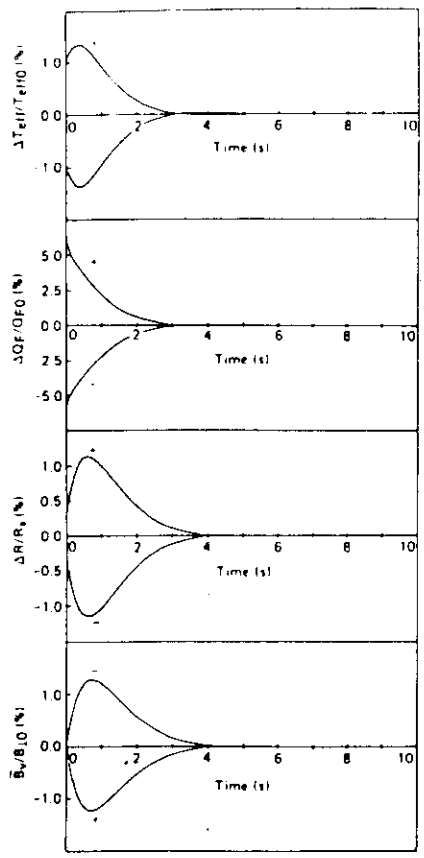

Fig. 4

Fig. 3 Transient responses of T_{eff}, Q_F, R, and B_V for T_{eff} control (G=2 and D=2 s). The + and - stand for the cases of positive and negative disturbances.

Fig. 4 Transient responses of T_{eff}, Q_F, R, and B_V for Q_F control (G=2 and D=2 s).

Reference for subsection 5.2

[1] L. Bromberg, J.L. Fisher, and D.R. Cohn, Nuclear Fusion 20 (1980) 203
[2] K. Borrass, Proc. 4th ANS Topl. Mtg. Technology of Controlled Nuclear Fusion, Pennsylvania (1980) 154
[3] M. Ohnishi, A. Saiki, and M. Okamoto, Nuclear Technology/Fusion 5 (1984) 326.

5.3 R and D programme

No contribution

5.4 Impact on INTOR design

No contribution

6. Plasma Diagnostics

No contribution